Pure and Applied Mathematics Quarterly
Volume 14, Number 1, 87–129, 2018

Accurate and efficient calculation of singular electrostatic potentials in charge-dielectric sphere systems

Caylah Retz and Wei Cai

Abstract: In this paper we introduce an efficient and accurate boundary element method for computing the electrostatic potential in closely-packed charge and dielectric spheres. A subtraction de-singularization technique is used to remove the singular part of the potential where the primary Coulomb potential and reaction field (approximated by image charges) are removed from the electrostatic potential. Regularization technique for the Hadamard finite part integral is also introduced for the second kind integral equations. Numerical results for one and two spheres have validated the effectiveness of the proposed method where much higher accuracy for the singular potential can be obtained with coarse meshes at a much reduced computational cost for closely packed charge-sphere systems.

Keywords: Poisson-Boltzmann equation, Dielectric sphere, charge.

1. Introduction

Electrostatic interactions are central to various applications: protein folding [23], ion transport, and colloidal material sciences [7, 1], to name a few. These processes and the solutions techniques to the posed mathematical systems have been investigated intensively. In general, the "solutions" we wish to procure is the electrostatic potential in space while the electric potential satisfies the Poisson and/or Poisson-Boltzmann (PB) partial differential equation [14].

Many different techniques for solving the Poisson-Boltzmann equation have been developed. Based on certain restrictions on computation time, or characteristics of the results, we have choices among a couple different approaches on how to mathematically frame our posed problem and relevant numerical methods. An analytical approach would mean generating solutions

Received March 28, 2018.
2010 Mathematics Subject Classification: 65R20, 65Z05, 78M25.

by, for example, image charge methods [8, 26, 13] or generalized Born approximations [24, 7]. A numerical approach would involve grid-based numerical methods, such as finite element methods (FEM's) [9–11, 15], finite difference methods [18, 22, 12], or boundary element methods [16, 4, 17, 6, 5, 22, 21]. Analytical approaches are attractive due to low computational cost. The downside, however, is that they are limited to special geometries. On the other side, numerical methods are more general, but their computational cost can be substantial. Research usually focuses on developing an acceptable balance between computational cost and accuracy.

A particular difficulty in solving the Poisson-Boltzmann equation emerges when the physical interaction desired to be modeled involves objects that are in close geometric proximity. In this scenery, the solution to the PB equation displays singular behavior that makes accurate calculation challenging. In designing solution techniques for the PB equation, efforts are made to push the threshold of minimum proximity distance while maintaining an acceptable level of accuracy for the electrostatic potential. It is our objective in this paper to improve the capability of boundary element methods to compute the electrostatic potential for close charge and sphere systems. The boundary integral equations reduce the dimension of our system by one compared to, for example, finite element methods [2, 3]. This reduction in dimension also reduces the computational cost and time of solving for the electrostatic potential.

We develop our methods to model the interaction of dielectric spheres and ion particles. The sphere is placed in a homogeneous medium. Our emphasis is on new techniques to calculate the electrostatic potential accurately when the ion is very close to the surface of the sphere. The paper is organized as follows. In Section 2, we introduce subtraction techniques to remove the singularity of the solution by a series of subtractions. In Section 3, a set of second kind boundary integrals equations (BIE) are derived for the desingularized potential for the sphere-ion system. Section 4 describes regularization techniques in computing Hadamard finite part of hypersingular integrals arising from the right hand side of the BIEs. Discretization of the BIEs and adaptive quadratures are given in Section 5. We extend the BIEs to a system of spheres in Section 6. Section 7 presents numerical tests to validate the effectiveness and accuracy of the proposed methods. Finally, a conclusion is given in Section 8.

2. Charge-sphere system and de-singularized potentials

Consider a sphere in an infinite as depicted in Fig. 1, homogeneous medium. For a region Ω_j, we denote its dielectric constants by ε_j and its inverse Debye

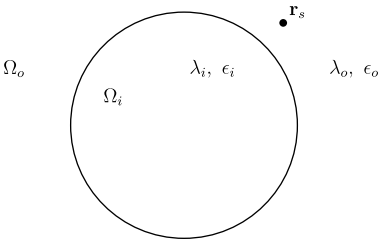

Figure 1: A system of one sphere and one charge.

Hückel lengths by λ_j. Here, Ω_o and Ω_i represents the domain outside and inside a spheroid, respectively. Similarly, the indices on the dielectric constants and inverse Debye-Hückel lengths indicate values inside and outside the sphere. Assume that there are is a charge with magnitude q_s at $\mathbf{r}_s$ located outside the sphere. For convenience, we let $q_s = 1$.

The potential field ϕ at arbitrary position $\mathbf{r}$ satisfies the Poisson-Boltzmann equation

$$\nabla^2\phi(\mathbf{r}) - \lambda^2(\mathbf{r})\phi(\mathbf{r}) = -\frac{4\pi}{\varepsilon(\mathbf{r})}q_s\delta(\mathbf{r}-\mathbf{r}_s) \tag{1}$$

with boundary conditions

$$[\phi(\mathbf{r})] = 0 \text{ and } \left[\varepsilon(\mathbf{r})\frac{\partial\phi(\mathbf{r})}{\partial\mathbf{n}}\right] = 0, \tag{2}$$

where δ is the Dirac delta function and $[\cdot]$ is the jump across the boundary. Here, we have

$$\varepsilon(\mathbf{r}) = \begin{cases} \varepsilon_i & \mathbf{r}\in\Omega_i \\ \varepsilon_o & \mathbf{r}\in\Omega_o \end{cases} \tag{3}$$

and

$$\lambda(\mathbf{r}) = \begin{cases} \lambda_i & \mathbf{r}\in\Omega_i \\ \lambda_o & \mathbf{r}\in\Omega_o \end{cases}. \tag{4}$$

Let the fundamental solution for (1) be denoted by G, where

$$G(\mathbf{r},\mathbf{r}') = \frac{e^{-\lambda|\mathbf{r}-\mathbf{r}'|}}{4\pi\varepsilon(\mathbf{r})|\mathbf{r}-\mathbf{r}'|}. \tag{5}$$

Then G satisfies the following PDE

$$\varepsilon(\mathbf{r})[\nabla^2 G(\mathbf{r},\mathbf{r}') - \lambda^2(\mathbf{r})G(\mathbf{r},\mathbf{r}')] = -\delta(\mathbf{r}-\mathbf{r}') \tag{6}$$

with the same boundary conditions in (2).

The potential $\phi(\mathbf{r})$ can be decomposed into two parts: a potential due to the source charge and a reaction field potential $\phi_{\text{rf}}(\mathbf{r})$ that reflects the polarization of the material outside the sphere, Ω_o, namely

$$\phi(\mathbf{r}) = \frac{q_s}{\varepsilon(\mathbf{r})|\mathbf{r}-\mathbf{r}_s|} + \phi_{\text{rf}}(\mathbf{r}). \tag{7}$$

Following the result in [8] and denoting the Kelvin image location at $\mathbf{x}_1$ and additional image charges at $\mathbf{x}_m$, we can estimate the reaction field potential using the multiple image charges as follows

$$\phi_{\text{rf}}(\mathbf{r}) \approx \frac{q_1}{\varepsilon(\mathbf{r})|\mathbf{r}-\mathbf{x}_1|} + \sum_{m=2}^{M-1} \frac{q_m}{\varepsilon(\mathbf{r})|\mathbf{r}-\mathbf{x}_m|}, \tag{8}$$

where M is a pre-determined number of image charge locations. The larger the M, the more accurate the estimation of the reaction field potential will be.

For practical applications where multiple spheres and charges are present, the electric potential $\phi(\mathbf{r})$ has no analytical solution and image approximations as above, and numerical methods are needed to find approximations. The main difficulty is that when a charge is very close to the surface of a sphere, the potential field becomes singular. In order to achieve better accuracy and efficiency in numerical approximation, we first define a "de-singularized" solution variable by subtracting the potential contribution due to the source charge in (7) as well as the dominant part of the field from the image charges (8). For this purpose, we define a function H by

$$H(\mathbf{r},\mathbf{r}_s) = 4\pi q_s G_o(\mathbf{r},\mathbf{r}_s), \tag{9}$$

where

$$G_o(\mathbf{r},\mathbf{r}_s) = \frac{e^{-\lambda_o|\mathbf{r}-\mathbf{r}_s|}}{4\pi\varepsilon_o|\mathbf{r}-\mathbf{r}_s|} \tag{10}$$

and where H satisfies the PB equation

$$\varepsilon_o[\nabla^2 H(\mathbf{r},\mathbf{r}_s) - \lambda_o^2 H(\mathbf{r},\mathbf{r}_s)] = -\rho(\mathbf{r}), \tag{11}$$

and, for sphere Ω,

$$\rho(\mathbf{r}) = \begin{cases} 4\pi q_s \delta(\mathbf{r}-\mathbf{r}_s) & \text{if } \mathbf{r} \in \Omega_o \\ 0 & \text{if } \mathbf{r} \in \Omega_i \end{cases}. \tag{12}$$

Secondly, define $T(\mathbf{r}, \mathbf{r}_s)$ equal to $n < M$ screened Coulomb potential terms as defined in [8],

$$T(\mathbf{r}, \mathbf{r}_s) = \frac{q_1 e^{-\lambda_o |\mathbf{r}-\mathbf{x}_1|}}{\varepsilon_o |\mathbf{r}-\mathbf{x}_1|} + \sum_{i=2}^{n} \frac{q_i e^{-\lambda_o |\mathbf{r}-\mathbf{x}_i|}}{\varepsilon_o |\mathbf{r}-\mathbf{x}_i|}, \tag{13}$$

where, for each image location $\mathbf{x}_i$, $T(\mathbf{r}, \mathbf{r}_s)$ satisfies the PB equation

$$\varepsilon_o [\nabla^2 T(\mathbf{r}, \mathbf{r}_s) - \lambda_o^2 T(\mathbf{r}, \mathbf{r}_s)] = -\nu(\mathbf{r}), \tag{14}$$

where

$$\nu(\mathbf{r}) = \begin{cases} 0 & \text{if } \mathbf{r} \in \Omega_o \\ 4\pi \sum_{i=1}^{n} q_i \delta(\mathbf{r}-\mathbf{x}_i) & \text{if } \mathbf{r} \in \Omega_i \end{cases}. \tag{15}$$

Next, we introduce a de-singularized solution variable w, to be used for the derivation of the boundary integral equation, as

$$w(\mathbf{r}) = \begin{cases} \phi_o(\mathbf{r}) - H(\mathbf{r}, \mathbf{r}_s) - T(\mathbf{r}, \mathbf{r}_s) & \text{if } \mathbf{r} \in \Omega_o \\ \phi_i(\mathbf{r}) & \text{if } \mathbf{r} \in \Omega_i \end{cases}, \tag{16}$$

which can be shown to satisfy a homogeneous PB equation in Ω_o and Ω_i, respectively, i.e.

$$\varepsilon_o (\nabla^2 w_o(\mathbf{r}) - \lambda_o^2 w_o(\mathbf{r})) = 0, \quad \mathbf{r} \in \Omega_o, \tag{17}$$

and

$$\varepsilon_i (\nabla^2 w_i(\mathbf{r}) - \lambda_{in}^2 w_i(\mathbf{r})) = 0, \quad \mathbf{r} \in \Omega_i.$$

We also have a new jump condition on the interface for w as

$$w_i - w_o = H + T,$$

and

$$\varepsilon_i \frac{\partial w_i}{\partial \mathbf{n}} - \varepsilon_o \frac{\partial w_o}{\partial \mathbf{n}} = \varepsilon_o \frac{\partial H(\mathbf{r}, \mathbf{r}_s)}{\partial \mathbf{n}} + \varepsilon_o \frac{\partial T(\mathbf{r}, \mathbf{r}_s)}{\partial \mathbf{n}}.$$

Namely, the boundary conditions for the de-singularized variable read

$$(18)\quad [w(\mathbf{r})] = H(\mathbf{r},\mathbf{r}_s)+T(\mathbf{r},\mathbf{r}_s),\ \left[\varepsilon(\mathbf{r})\frac{\partial w(\mathbf{r})}{\partial \mathbf{n}}\right] = \varepsilon_o\frac{\partial H(\mathbf{r},\mathbf{r}_s)}{\partial \mathbf{n}}+\varepsilon_o\frac{\partial T(\mathbf{r},\mathbf{r}_s)}{\partial \mathbf{n}}.$$

3. Boundary integral equations

3.1. Integral equations of the first kind

Recall that the fundamental solution to the Poisson-Boltzmann equation in a homogeneous medium is given by

$$G(\mathbf{r},\mathbf{r}') = \frac{e^{-\lambda(\mathbf{r})|\mathbf{r}-\mathbf{r}'|}}{4\pi\varepsilon(\mathbf{r})|\mathbf{r}-\mathbf{r}'|}.$$

The boundary integral equations are derived from inside and outside the boundary of the sphere, thus the values of $\varepsilon(\mathbf{r})$ and $\lambda(\mathbf{r})$ change, accordingly. $G_i(\mathbf{r},\mathbf{r}')$ and $G_o(\mathbf{r},\mathbf{r}')$ indicate the corresponding fundamental solution for the media inside and outside the sphere, respectively.

Now, consider an observation point $\mathbf{r}'$ located outside the boundary of the sphere. Then we have

$$(19)\quad \varepsilon_o\left(\nabla^2 w_o(\mathbf{r}) - \lambda_o^2 w_o(\mathbf{r})\right) = 0$$

$$(20)\quad \varepsilon_o(\nabla^2 G_o(\mathbf{r},\mathbf{r}') - \lambda_o^2 G_o(\mathbf{r},\mathbf{r}')) = -\delta(\mathbf{r}-\mathbf{r}')$$

We multiply (19) by $G_o(\mathbf{r},\mathbf{r}')$ and (20) by $w_o(\mathbf{r})$, take their difference, and integrate over the exterior of Ω and a ball $B(\mathbf{r}',\rho)$ of radius ρ centered at $\mathbf{r}'$. If we let $D_1 = R^3\setminus(\Omega\cup B(\mathbf{r}',\rho))$ be this integration domain and S represent the surface of the dielectric sphere, we then have

$$\int_{D_1} \varepsilon_o(G_o(\mathbf{r},\mathbf{r}')\nabla^2 w_o(\mathbf{r}) - w_o(\mathbf{r})\nabla^2 G_o(\mathbf{r},\mathbf{r}'))\,\mathrm{d}\mathbf{r} = \int_{D_1} w_o(\mathbf{r})\delta(\mathbf{r}-\mathbf{r}')\,\mathrm{d}\mathbf{r},$$

then

$$(21)\quad \int_{D_1} \varepsilon_o(G_o(\mathbf{r},\mathbf{r}')\nabla^2 w_o(\mathbf{r}) - w_o(\mathbf{r})\nabla^2 G_o(\mathbf{r},\mathbf{r}'))\,\mathrm{d}\mathbf{r} = 0.$$

Then by a familiar application of Green's second identity, we have

$$(22)\quad \oint_{\partial D_1} \varepsilon_o\left(G_o(\mathbf{r},\mathbf{r}')\frac{\partial w_o(\mathbf{r})}{\partial \mathbf{n}} - w_o(\mathbf{r})\frac{\partial G_o(\mathbf{r},\mathbf{r}')}{\partial \mathbf{n}}\right)\mathrm{d}S(\mathbf{r}) = 0.$$

Next, we integrate over the separate parts of the boundary to obtain

$$\oint_S \varepsilon_o \left(w_o(\mathbf{r}) \frac{\partial G_o(\mathbf{r}, \mathbf{r}')}{\partial \mathbf{n}} - G_o(\mathbf{r}, \mathbf{r}') \frac{\partial w_o(\mathbf{r})}{\partial \mathbf{n}} \right) \mathrm{d}S(\mathbf{r}) + (-w_o(\mathbf{r}')) = 0$$

$$w_o(\mathbf{r}') = \oint_S \varepsilon_o \left(w_o(\mathbf{r}) \frac{\partial G_o(\mathbf{r}, \mathbf{r}')}{\partial \mathbf{n}} - G_o(\mathbf{r}, \mathbf{r}') \frac{\partial w_o(\mathbf{r})}{\partial \mathbf{n}} \right) \mathrm{d}S(\mathbf{r}). \tag{23}$$

Letting $\mathbf{r}'$ approach point $\mathbf{p}$ on the surface of the sphere, we have

$$\frac{1}{2} w_o(\mathbf{p}) = \oint_S \varepsilon_o \left(w_o(\mathbf{r}) \frac{\partial G_o(\mathbf{r}, \mathbf{p})}{\partial \mathbf{n}} - G_o(\mathbf{r}, \mathbf{p}) \frac{\partial w_o(\mathbf{r})}{\partial \mathbf{n}} \right) \mathrm{d}S(\mathbf{r}). \tag{24}$$

Similarly, now consider observation point $\mathbf{r}'$ located inside the boundary of the sphere. Then just as before, the two partial differential equations for the region on the interior of the sphere are:

$$\varepsilon_i (\nabla^2 w_i(\mathbf{r}) - \lambda_i^2 w_i(\mathbf{r})) = 0 \tag{25}$$

$$\varepsilon_i (\nabla^2 G_i(\mathbf{r}, \mathbf{r}') - \lambda_i^2 G_i(\mathbf{r}, \mathbf{r}')) = -\delta(\mathbf{r} - \mathbf{r}'). \tag{26}$$

We then multiply (25) by $G_i(\mathbf{r}, \mathbf{r}')$ and (26) by $w_i(\mathbf{r})$ and integrate their difference over $D_2 = \Omega \setminus B(\mathbf{r}', \rho)$ to obtain

$$\int_{D_2} \varepsilon_i (G_i(\mathbf{r}, \mathbf{r}') \nabla^2 w_i(\mathbf{r}) - w_i(\mathbf{r}) \nabla^2 G_i(\mathbf{r}, \mathbf{r}')) \, \mathrm{d}\mathbf{r} = \int_{D_2} w_i(\mathbf{r}) \delta(\mathbf{r} - \mathbf{r}') \, \mathrm{d}\mathbf{r} = 0, \tag{27}$$

where $B(\mathbf{r}', \rho)$ is a ball of radius ρ at $\mathbf{r}'$. Again we apply Green's second identity and move the integral to the boundary S and take the limit as ρ goes to zero.

$$w_i(\mathbf{r}') = \oint_S \varepsilon_i \left(G_i(\mathbf{r}, \mathbf{r}') \frac{\partial w_i(\mathbf{r})}{\partial \mathbf{n}} - w_i(\mathbf{r}) \frac{\partial G_i(\mathbf{r}, \mathbf{r}')}{\partial \mathbf{n}} \right) \mathrm{d}S(\mathbf{r}) \tag{28}$$

Taking the limit as $\mathbf{r}'$ approaches a point $\mathbf{p}$ in S from the inside,

$$\frac{1}{2} w_i(\mathbf{p}) = \oint_S \varepsilon_i \left(G_i(\mathbf{r}, \mathbf{p}) \frac{\partial w_i(\mathbf{r})}{\partial \mathbf{n}} - w_i(\mathbf{r}) \frac{\partial G_i(\mathbf{r}, \mathbf{p})}{\partial \mathbf{n}} \right) \mathrm{d}S(\mathbf{r}),$$

which can be rewritten in terms of the smoother quantity $w_o(\mathbf{p})$ using the jump conditions (18):

$$\begin{aligned}
&\frac{1}{2}(w_o(\mathbf{p}) + H(\mathbf{p},\mathbf{r}_s) + T(\mathbf{p},\mathbf{r}_s)) \\
&= \oint_S \varepsilon_i \left[G_i(\mathbf{r},\mathbf{p}) \left(\frac{\varepsilon_o}{\varepsilon_i} \frac{\partial H(\mathbf{r},\mathbf{r}_s)}{\partial \mathbf{n}} + \frac{\varepsilon_o}{\varepsilon_i} \frac{\partial w_o(\mathbf{r})}{\partial \mathbf{n}} + \frac{\varepsilon_o}{\varepsilon_i} \frac{\partial T(\mathbf{r},\mathbf{r}_s)}{\partial \mathbf{n}} \right) \right. \\
&\left. -(w_o(\mathbf{r}) + H(\mathbf{r},\mathbf{r}_s) + T(\mathbf{r},\mathbf{r}_s)) \frac{\partial G_i(\mathbf{r},\mathbf{p})}{\partial \mathbf{n}} \right] \mathrm{d}S(\mathbf{r}), \qquad (29)
\end{aligned}$$

re-written as

$$\begin{aligned}
&\frac{1}{2} w_o(\mathbf{p}) - \oint_S \left(\varepsilon_o G_i(\mathbf{r},\mathbf{p}) \frac{\partial w_o(\mathbf{r})}{\partial \mathbf{n}} - \varepsilon_i w_o(\mathbf{r}) \frac{\partial G_i(\mathbf{r},\mathbf{p})}{\partial \mathbf{n}} \right) \mathrm{d}S(\mathbf{r}) \\
&= \oint_S \left(\varepsilon_o G_i(\mathbf{r},\mathbf{p}) \frac{\partial H(\mathbf{r},\mathbf{r}_s)}{\partial \mathbf{n}} - \varepsilon_i H(\mathbf{r},\mathbf{r}_s) \frac{\partial G_i(\mathbf{r},\mathbf{p})}{\partial \mathbf{n}} \right) \mathrm{d}S(\mathbf{r}) \\
&+ \oint_S \left(\varepsilon_o G_i(\mathbf{r},\mathbf{p}) \frac{\partial T(\mathbf{r},\mathbf{r}_s)}{\partial \mathbf{n}} - \varepsilon_i T(\mathbf{r},\mathbf{r}_s) \frac{\partial G_i(\mathbf{r},\mathbf{p})}{\partial \mathbf{n}} \right) \mathrm{d}S(\mathbf{r}) \\
&- \frac{1}{2} H(\mathbf{p},\mathbf{r}_s) - \frac{1}{2} T(\mathbf{p},\mathbf{r}_s). \qquad (30)
\end{aligned}$$

Together equations (24) and (30) make up the integral equations of the first kind. However, they form an ill-conditioned system of equations [7] [28], and we consider integral equations of the second kind instead in the next section.

3.2. Integral equations of the second kind

The first equation of the second kind is formed by taking the sum of equations (24) and (30). The second equation of the second kind is formed by the sum of the derivatives of (24) and (30) [16][28]. First, we find the normal derivative of the boundary integral equation outside the sphere before we took the limit as $\mathbf{r}' \to \mathbf{p}$. That is, taking the derivative of (23) with respect to $\mathbf{r}'$, we get the following equation for when $\mathbf{r}'$ is outside of Ω:

$$\frac{\partial w_o(\mathbf{r}')}{\partial \mathbf{n}'} = \oint_S \varepsilon_o \left(w_o(\mathbf{r}) \frac{\partial^2 G_o(\mathbf{r},\mathbf{r}')}{\partial \mathbf{n}' \partial \mathbf{n}} - \frac{\partial G_o(\mathbf{r},\mathbf{r}')}{\partial \mathbf{n}'} \frac{\partial w_o(\mathbf{r})}{\partial \mathbf{n}} \right) \mathrm{d}S(\mathbf{r}). \qquad (31)$$

Taking the limit from the outside as $\mathbf{r}'$ approaches a point $\mathbf{p}$ in S, we have

$$\frac{1}{2}\frac{\partial w_o(\mathbf{p})}{\partial \mathbf{n}} = \oint_S \varepsilon_o \left(w_o(\mathbf{r}) \frac{\partial^2 G_o(\mathbf{r},\mathbf{p})}{\partial \mathbf{n}' \partial \mathbf{n}} - \frac{\partial G_o(\mathbf{r},\mathbf{p})}{\partial \mathbf{n}'} \frac{\partial w_o(\mathbf{r})}{\partial \mathbf{n}} \right) \mathrm{d}S(\mathbf{r}). \tag{32}$$

Secondly, we take the normal derivative of the boundary integral equation inside the sphere from before the limiting equation was obtained to yield

$$\frac{\partial w_i(\mathbf{r}')}{\partial \mathbf{n}'} = \oint_S \varepsilon_i \left(\frac{\partial G_i(\mathbf{r},\mathbf{r}')}{\partial \mathbf{n}'} \frac{\partial w_i(\mathbf{r})}{\partial \mathbf{n}} - w_i(\mathbf{r}) \frac{\partial^2 G_i(\mathbf{r},\mathbf{r}')}{\partial \mathbf{n}' \partial \mathbf{n}} \right) \mathrm{d}S(\mathbf{r}). \tag{33}$$

By taking the limit as $\mathbf{r}'$ approaches a point $\mathbf{p}$ in S from the inside, we have

$$\frac{1}{2}\frac{w_i(\mathbf{p})}{\partial \mathbf{n}} = \oint_S \varepsilon_i \left(\frac{\partial G_i(\mathbf{r},\mathbf{p})}{\partial \mathbf{n}'} \frac{\partial w_i(\mathbf{r})}{\partial \mathbf{n}} - w_i(\mathbf{r}) \frac{\partial^2 G_i(\mathbf{r},\mathbf{p})}{\partial \mathbf{n}' \partial \mathbf{n}} \right) \mathrm{d}S(\mathbf{r}),$$

which can be rewritten in terms of the smoother variable w_o via the jump conditions (18),

$$\begin{aligned} &\frac{1}{2}\frac{\varepsilon_o}{\varepsilon_i}\left(\frac{\partial H(\mathbf{p},\mathbf{r}_s)}{\partial \mathbf{n}} + \frac{\partial w_o(\mathbf{p})}{\partial \mathbf{n}} + \frac{\partial T(\mathbf{p},\mathbf{r}_s)}{\partial \mathbf{n}} \right) \\ &= \oint_S \varepsilon_i \frac{\partial G_i(\mathbf{r},\mathbf{p})}{\partial \mathbf{n}'} \left(\frac{\varepsilon_o}{\varepsilon_i} \frac{\partial H(\mathbf{r},\mathbf{r}_s)}{\partial \mathbf{n}} + \frac{\varepsilon_o}{\varepsilon_i} \frac{\partial w_o(\mathbf{r})}{\partial \mathbf{n}} + \frac{\varepsilon_o}{\varepsilon_i} \frac{\partial T(\mathbf{r},\mathbf{r}_s)}{\partial \mathbf{n}} \right) \mathrm{d}S(\mathbf{r}) \\ &- \oint_S \varepsilon_i (w_o(\mathbf{r}) + H(\mathbf{r},\mathbf{r}_s) + T(\mathbf{r},\mathbf{r}_s)) \frac{\partial^2 G_i(\mathbf{r},\mathbf{p})}{\partial \mathbf{n}' \partial \mathbf{n}} \mathrm{d}S(\mathbf{r}), \end{aligned} \tag{34}$$

so that by rearranging,

$$\begin{aligned} \frac{1}{2}\frac{\varepsilon_o}{\varepsilon_i}\frac{\partial w_o(\mathbf{p})}{\partial \mathbf{n}} &= \oint_S \left(\varepsilon_o \frac{\partial G_i(\mathbf{r},\mathbf{p})}{\partial \mathbf{n}'} \frac{\partial w_o(\mathbf{r})}{\partial \mathbf{n}} - \varepsilon_i w_o(\mathbf{r}) \frac{\partial^2 G_i(\mathbf{r},\mathbf{p})}{\partial \mathbf{n}' \partial \mathbf{n}} \right) \mathrm{d}S(\mathbf{r}) \\ &+ \oint_S \left(\varepsilon_o \frac{\partial G_i(\mathbf{r},\mathbf{p})}{\partial \mathbf{n}'} \frac{\partial H(\mathbf{r},\mathbf{r}_s)}{\partial \mathbf{n}} - \varepsilon_i H(\mathbf{r},\mathbf{r}_s) \frac{\partial^2 G_i(\mathbf{r},\mathbf{p})}{\partial \mathbf{n}' \partial \mathbf{n}} \right) \mathrm{d}S(\mathbf{r}) \\ &+ \oint_S \left(\varepsilon_o \frac{\partial G_i(\mathbf{r},\mathbf{p})}{\partial \mathbf{n}'} \frac{\partial T(\mathbf{r},\mathbf{r}_s)}{\partial \mathbf{n}} - \varepsilon_i T(\mathbf{r},\mathbf{r}_s) \frac{\partial^2 G_i(\mathbf{r},\mathbf{p})}{\partial \mathbf{n}' \partial \mathbf{n}} \right) \mathrm{d}S(\mathbf{r}) \\ &- \frac{1}{2}\frac{\varepsilon_o}{\varepsilon_i}\frac{\partial H(\mathbf{p},\mathbf{r}_s)}{\partial \mathbf{n}} - \frac{1}{2}\frac{\varepsilon_o}{\varepsilon_i}\frac{\partial T(\mathbf{p},\mathbf{r}_s)}{\partial \mathbf{n}}. \end{aligned} \tag{35}$$

Now, the first integral equation of the second kind is the sum of (24) and (30):

$$
\begin{aligned}
w_o(\mathbf{p}) &- \oint_S \varepsilon_o \left(G_i(\mathbf{r},\mathbf{p}) - G_o(\mathbf{r},\mathbf{p})\right) \frac{\partial w_o(\mathbf{r})}{\partial \mathbf{n}}\, \mathrm{d}S(\mathbf{r}) \\
&- \oint_S \left(\varepsilon_o \frac{\partial G_o(\mathbf{r},\mathbf{p})}{\partial \mathbf{n}} - \varepsilon_i \frac{\partial G_i(\mathbf{r},\mathbf{p})}{\partial \mathbf{n}}\right) w_o(\mathbf{r})\, \mathrm{d}S(\mathbf{r}) \\
&= \oint_S \left(\varepsilon_o G_i(\mathbf{r},\mathbf{p}) \frac{\partial H(\mathbf{r},\mathbf{r}_s)}{\partial \mathbf{n}} - \varepsilon_i H(\mathbf{r},\mathbf{r}_s) \frac{G_i(\mathbf{r},\mathbf{p})}{\partial \mathbf{n}}\right) \mathrm{d}S(\mathbf{r}) \\
&+ \oint_S \left(\varepsilon_o G_i(\mathbf{r},\mathbf{p}) \frac{\partial T(\mathbf{r},\mathbf{r}_s)}{\partial \mathbf{n}} - \varepsilon_i T(\mathbf{r},\mathbf{r}_s) \frac{\partial G_i(\mathbf{r},\mathbf{p})}{\partial \mathbf{n}}\right) \mathrm{d}S(\mathbf{r}) \\
&- \frac{1}{2} H(\mathbf{p},\mathbf{r}_s) - \frac{1}{2} T(\mathbf{p},\mathbf{r}_s).
\end{aligned} \tag{36}
$$

The second equation is the sum of (32) and (35):

$$
\begin{aligned}
&\left(\frac{1}{2} + \frac{1}{2}\frac{\varepsilon_o}{\varepsilon_i}\right) \frac{\partial w_o(\mathbf{p})}{\partial \mathbf{n}} - \oint_S \left(\varepsilon_o \frac{\partial^2 G_o(\mathbf{r},\mathbf{p})}{\partial \mathbf{n}' \partial \mathbf{n}} - \varepsilon_i \frac{\partial^2 G_i(\mathbf{r},\mathbf{p})}{\partial \mathbf{n}' \partial \mathbf{n}}\right) w_o(\mathbf{r})\, \mathrm{d}S(\mathbf{r}) \\
&- \oint_S \left(\varepsilon_o \frac{\partial G_i(\mathbf{r},\mathbf{p})}{\partial \mathbf{n}'} - \varepsilon_o \frac{\partial G_o(\mathbf{r},\mathbf{p})}{\partial \mathbf{n}'}\right) \frac{\partial w_o(\mathbf{r})}{\partial \mathbf{n}}\, \mathrm{d}S(\mathbf{r}) \\
&= -\text{p.f.} \oint_S \varepsilon_i \left(H(\mathbf{r},\mathbf{r}_s) + T(\mathbf{r},\mathbf{r}_s)\right) \frac{\partial^2 G_i(\mathbf{r},\mathbf{p})}{\partial \mathbf{n}' \partial \mathbf{n}}\, \mathrm{d}S(\mathbf{r}) \\
&+ \oint_S \varepsilon_o \frac{\partial H(\mathbf{r},\mathbf{r}_s)}{\partial \mathbf{n}} \frac{\partial G_i(\mathbf{r},\mathbf{p})}{\partial \mathbf{n}'}\, \mathrm{d}S(\mathbf{r}) + \oint_S \varepsilon_o \frac{\partial T(\mathbf{r},\mathbf{r}_s)}{\partial \mathbf{n}} \frac{\partial G_i(\mathbf{r},\mathbf{p})}{\partial \mathbf{n}'}\, \mathrm{d}S(\mathbf{r}) \\
&- \frac{1}{2}\frac{\varepsilon_o}{\varepsilon_i} \frac{\partial H(\mathbf{p},\mathbf{r}_s)}{\partial \mathbf{n}} - \frac{1}{2}\frac{\varepsilon_o}{\varepsilon_i} \frac{\partial T(\mathbf{p},\mathbf{r}_s)}{\partial \mathbf{n}}.
\end{aligned} \tag{37}
$$

The hypersingular integrals in (37) need regularization so that they can be accurately calculated for source charges very close to the boundary of the sphere.

4. Regularization of hypersingular integrals

The integrals involved in (32) and (37) become difficult to calculate when $\mathbf{r}$ is close to $\mathbf{p}$ or when $\mathbf{r}$ is close to $\mathbf{r}_s$, due to the $\mathrm{O}(\frac{1}{|\mathbf{r}-\mathbf{r}'|})$ singularity of the

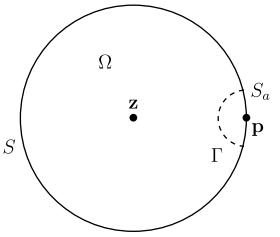

Figure 2: Sphere and hemisphere setup for mesh point **p**.

Green's function $G(\mathbf{r},\mathbf{r}')$. This difficulty is even worse as some of the integrals in the BIEs contain the second derivative of $G(\mathbf{r},\mathbf{r}')$. In fact, $\frac{\partial^2 G(\mathbf{r},\mathbf{r}')}{\partial \mathbf{n}\partial \mathbf{n}'}$ displays singular behavior of order $\mathrm{O}\Big(\frac{1}{|\mathbf{r}-\mathbf{r}'|^3}\Big)$. To mitigate the difficulty encountered in calculation, we introduce a method to reduce the order of the singularity in this hypersingular integrals. Let Σ denote the Hadamard finite part of the hypersingular integral of interest, namely

$$\Sigma = -\text{p.f.} \oint_S \varepsilon_i (H(\mathbf{r},\mathbf{r}_s) + T(\mathbf{r},\mathbf{r}_s)) \frac{\partial^2 G_i(\mathbf{r},\mathbf{p})}{\partial \mathbf{n}'\partial \mathbf{n}} \,\mathrm{d}S(\mathbf{r}). \tag{38}$$

4.1. A small hemisphere Γ and special solution $v(\mathbf{r})$

To compute the Hadamard finite part, let us introduce a mathematical boundary on our sphere-particle physical setup and boundary [27]. Construct a hemisphere of radius a centering at the point **p** along the inside of the surface of our sphere (refer to Figure 2). The hemispherical surface is denoted by Γ and the intersection of the hemisphere and the boundary of Ω is denoted by $S_a \equiv S_a(\mathbf{p})$. We call the region enclosed by this hemisphere Ω_p.

For some $\mathbf{z} \in \Omega_i,\ \mathbf{z} \notin \Omega_p$ and for some appropriately chosen constant C, we consider a special solution for the potential of a charge at **z** located in the center of the bigger sphere:

$$v(\mathbf{r}) = C \frac{e^{-\lambda(\mathbf{r})|\mathbf{r}-\mathbf{z}|}}{\varepsilon(\mathbf{r})|\mathbf{r}-\mathbf{z}|}. \tag{39}$$

Then $v(\mathbf{r})$ satisfies the following PDE

$$\varepsilon(\mathbf{r})(\nabla^2 v(\mathbf{r}) - \lambda^2(\mathbf{r}) v(\mathbf{r})) = -C \cdot 4\pi\delta(\mathbf{r}-\mathbf{z}). \tag{40}$$

Given the radius r of the sphere Ω, if we impose the restriction for the hemisphere that $a < \frac{1}{2}r$, then the PDE for $v(\mathbf{r})$ in Ω_p is given by

$$\varepsilon_i(\nabla^2 v(\mathbf{r}) - \lambda_i^2 v(\mathbf{r})) = 0. \tag{41}$$

Using the Green's function $G_i(\mathbf{r}, \mathbf{r}')$ for the domain Ω_p defined by

$$\varepsilon_i(\nabla^2 G_i(\mathbf{r}, \mathbf{r}') - \lambda_i^2 G_i(\mathbf{r}, \mathbf{r}')) = -\delta(\mathbf{r} - \mathbf{r}'),$$

the solution $v(\mathbf{r})$ has the following integral representation for $\mathbf{r}'$

$$\begin{aligned} v(\mathbf{r}') = &\oint_{S_a} \varepsilon_i \left(G_i(\mathbf{r}, \mathbf{r}') \frac{\partial v(\mathbf{r})}{\partial \mathbf{n}_o} - v(\mathbf{r}) \frac{\partial G_i(\mathbf{r}, \mathbf{r}')}{\partial \mathbf{n}_o} \right) \mathrm{d}S(\mathbf{r}) \\ &+ \oint_{\Gamma} \varepsilon_i \left(G_i(\mathbf{r}, \mathbf{r}') \frac{\partial v(\mathbf{r})}{\partial \mathbf{n}_\Gamma} - v(\mathbf{r}) \frac{\partial G_i(\mathbf{r}, \mathbf{r}')}{\partial \mathbf{n}_\Gamma} \right) \mathrm{d}S(\mathbf{r}). \end{aligned} \tag{42}$$

Next, taking the normal derivative of (42) with respect to $\mathbf{r}'$,

$$\begin{aligned} \frac{\partial v(\mathbf{r}')}{\partial \mathbf{n}_o'} = &\oint_{S_a} \varepsilon_i \left(\frac{\partial G_i(\mathbf{r}, \mathbf{r}')}{\partial \mathbf{n}_o'} \frac{\partial v(\mathbf{r})}{\partial \mathbf{n}_o} - v(\mathbf{r}) \frac{\partial^2 G_i(\mathbf{r}, \mathbf{r}')}{\partial \mathbf{n}_o' \partial \mathbf{n}_o} \right) \mathrm{d}S(\mathbf{r}) \\ &+ \oint_{\Gamma} \varepsilon_i \left(\frac{\partial G_i(\mathbf{r}, \mathbf{r}')}{\partial \mathbf{n}_o'} \frac{\partial v(\mathbf{r})}{\partial \mathbf{n}_\Gamma} - v(\mathbf{r}) \frac{\partial^2 G_i(\mathbf{r}, \mathbf{r}')}{\partial \mathbf{n}_o' \partial \mathbf{n}_\Gamma} \right) \mathrm{d}S(\mathbf{r}), \end{aligned} \tag{43}$$

and taking the limit as $\mathbf{r}'$ approaches $\mathbf{p}$ in S from the inside yields the identity

$$\begin{aligned} \frac{1}{2} \frac{\partial v(\mathbf{p})}{\partial \mathbf{n}_o} - &\oint_{S_a} \varepsilon_i \left(\frac{\partial G_i(\mathbf{r}, \mathbf{p})}{\partial \mathbf{n}_o'} \frac{\partial v(\mathbf{r})}{\partial \mathbf{n}_o} - v(\mathbf{r}) \frac{\partial^2 G_i(\mathbf{r}, \mathbf{p})}{\partial \mathbf{n}_o' \partial \mathbf{n}_o} \right) \mathrm{d}S(\mathbf{r}) \\ &- \oint_{\Gamma} \varepsilon_i \left(\frac{\partial G_i(\mathbf{r}, \mathbf{p})}{\partial \mathbf{n}_o'} \frac{\partial v(\mathbf{r})}{\partial \mathbf{n}_\Gamma} - v(\mathbf{r}) \frac{\partial^2 G_i(\mathbf{r}, \mathbf{p})}{\partial \mathbf{n}_o' \partial \mathbf{n}_\Gamma} \right) \mathrm{d}S(\mathbf{r}) = 0. \end{aligned} \tag{44}$$

4.2. De-singularized Hadamard finite part and modified boundary integral equations

We now treat (44) as the value zero and add it to our hyper-singular integral Σ in (38). But first let us split Σ up over the union of its domain $(S \setminus S_a) \cup S_a$ and use the above identity. Then

$$\Sigma = - \oint_{(S \setminus S_a)} \varepsilon_i (H(\mathbf{r}, \mathbf{r}_s) + T(\mathbf{r}, \mathbf{r}_s)) \frac{\partial^2 G_i(\mathbf{r}, \mathbf{p})}{\partial \mathbf{n}_o' \partial \mathbf{n}_o} \mathrm{d}S(\mathbf{r}) \tag{45}$$

$$-\oint_{S_a} \varepsilon_i (H(\mathbf{r},\mathbf{r}_s)+T(\mathbf{r},\mathbf{r}_s)) \frac{\partial^2 G_i(\mathbf{r},\mathbf{p})}{\partial \mathbf{n}'_o \partial \mathbf{n}_o}\,\mathrm{d}S(\mathbf{r}). \tag{46}$$

Adding 0 as (44) to Σ:

$$\begin{aligned}
\Sigma + 0 = &-\oint_{(S\ S_a)} \varepsilon_i (H(\mathbf{r},\mathbf{r}_s)+T(\mathbf{r},\mathbf{r}_s)) \frac{\partial^2 G_i(\mathbf{r},\mathbf{p})}{\partial \mathbf{n}'_o \partial \mathbf{n}_o}\,\mathrm{d}S(\mathbf{r}) \\
&+\oint_{S_a} \varepsilon_i \left(v(\mathbf{r})-H(\mathbf{r},\mathbf{r}_s)-T(\mathbf{r},\mathbf{r}_s)\right) \frac{\partial^2 G_i(\mathbf{r},\mathbf{p})}{\partial \mathbf{n}'_o \partial \mathbf{n}_o}\,\mathrm{d}S(\mathbf{r}) \\
&-\oint_{S_a} \varepsilon_i \left(\frac{\partial G_i(\mathbf{r},\mathbf{p})}{\partial \mathbf{n}'_o}\frac{\partial v(\mathbf{r})}{\partial \mathbf{n}_o}\right)\mathrm{d}S(\mathbf{r}) - \oint_{\Gamma} \varepsilon_i \left(\frac{\partial G_i(\mathbf{r},\mathbf{p})}{\partial \mathbf{n}'_o}\frac{\partial v(\mathbf{r})}{\partial \mathbf{n}_\Gamma}\right)\mathrm{d}S(\mathbf{r}) \\
&+\oint_{\Gamma} \varepsilon_i \left(v(\mathbf{r})\frac{\partial^2 G_i(\mathbf{r},\mathbf{p})}{\partial \mathbf{n}'_o \partial \mathbf{n}_\Gamma}\right)\mathrm{d}S(\mathbf{r}) + \frac{1}{2}\frac{\partial v(\mathbf{p})}{\partial \mathbf{n}_o}.
\end{aligned} \tag{47}$$

It can be shown using Taylor series that $v(\mathbf{r}) - H(\mathbf{r},\mathbf{r}_s) - T(\mathbf{r},\mathbf{r}_s) = O(|\mathbf{r}-\mathbf{p}|)$ as $\mathbf{r}$ goes to $\mathbf{p}$ (refer to the appendix). Now, the second integral in (47) is of order $\mathrm{O}\left(\frac{1}{|\mathbf{r}-\mathbf{p}|^2}\right)$. We can then replace Σ in (37) with these additional integrals. We should note that the whole purpose of introducing the special solution $v(\mathbf{r})$ is to introduce the $v(\mathbf{r}) - H(\mathbf{r},\mathbf{r}_s) - T(\mathbf{r},\mathbf{r}_s)$ subtraction in the second integral in (47) for a reduction in singularity order. Further, we can see now that the constant C should be chosen so that $v(\mathbf{r}) - H(\mathbf{r},\mathbf{r}_s) - T(\mathbf{r},\mathbf{r}_s)$ vanishes at a point $\mathbf{p}$ on the surface of the sphere. Finally, equation (35) can be re-written as

$$\begin{aligned}
&\frac{1}{2}\frac{\varepsilon_o}{\varepsilon_i}\frac{\partial w_o(\mathbf{p})}{\partial \mathbf{n}'_o} - \oint_S \left(\varepsilon_o \frac{\partial G_i(\mathbf{r},\mathbf{p})}{\partial \mathbf{n}'_o}\frac{\partial w_o(\mathbf{r})}{\partial \mathbf{n}_o} - \varepsilon_i w_o(\mathbf{r})\frac{\partial^2 G_i(\mathbf{r},\mathbf{p})}{\partial \mathbf{n}'_o \partial \mathbf{n}_o}\right)\mathrm{d}S(\mathbf{r}) \\
&= \oint_S \varepsilon_o \frac{\partial G_i(\mathbf{r},\mathbf{p})}{\partial \mathbf{n}'_o}\left(\frac{\partial H(\mathbf{r},\mathbf{r}_s)}{\partial \mathbf{n}_o}+\frac{\partial T(\mathbf{r},\mathbf{r}_s)}{\partial \mathbf{n}_o}\right)\mathrm{d}S(\mathbf{r}) \\
&\quad -\oint_{S\setminus S_a} \varepsilon_i (H(\mathbf{r},\mathbf{r}_s)+T(\mathbf{r},\mathbf{r}_s)) \frac{\partial^2 G_i(\mathbf{r},\mathbf{p})}{\partial \mathbf{n}'_o \partial \mathbf{n}_o}\,\mathrm{d}S(\mathbf{r}) \\
&\quad +\oint_{S_a} \varepsilon_i (v(\mathbf{r})-H(\mathbf{r},\mathbf{r}_s)-T(\mathbf{r},\mathbf{r}_s)) \frac{\partial^2 G_i(\mathbf{r},\mathbf{p})}{\partial \mathbf{n}'_o \partial \mathbf{n}_o}\,\mathrm{d}S(\mathbf{r}) \\
&\quad +\oint_{\Gamma} \varepsilon_i v(\mathbf{r}) \frac{\partial^2 G_i(\mathbf{r},\mathbf{p})}{\partial \mathbf{n}'_o \partial \mathbf{n}_\Gamma}\,\mathrm{d}S(\mathbf{r}) - \oint_{S_a} \varepsilon_i \frac{\partial G_i(\mathbf{r},\mathbf{p})}{\partial \mathbf{n}'_o}\frac{\partial v(\mathbf{r})}{\partial \mathbf{n}_o}\,\mathrm{d}S(\mathbf{r})
\end{aligned}$$

$$
\begin{aligned}
&- \oint_{\Gamma} \varepsilon_i \frac{\partial G_i(\mathbf{r},\mathbf{p})}{\partial \mathbf{n}_o} \frac{\partial v(\mathbf{r})}{\partial \mathbf{n}_\Gamma} \,\mathrm{d}S(\mathbf{r}) + \frac{1}{2}\frac{\partial v(\mathbf{p})}{\partial \mathbf{n}_o} \\
&- \frac{1}{2}\frac{\varepsilon_o}{\varepsilon_i}\frac{\partial H(\mathbf{p},\mathbf{r}_s)}{\partial \mathbf{n}} - \frac{1}{2}\frac{\varepsilon_o}{\varepsilon_i}\frac{\partial T(\mathbf{p},\mathbf{r}_s)}{\partial \mathbf{n}}.
\end{aligned} \tag{48}
$$

5. Discretized equations and adaptive quadratures

To solve the boundary integral equations, we discretize the boundary S by introducing a mesh of curvilinear triangles that conform to our surface [19][28] and satisfy the integral equations (36) and (48) at selected nodes in each triangular mesh [5], resulting in a matrix equation.

5.1. Matrix equation

Let $\mathbf{r}_t$ denote the coordinates of the t^{th} mesh point, and let $\psi(\mathbf{r})$ represent basis functions with the Kronecker delta property, $\psi_{t_i}(\mathbf{r}_{t_j}) = \delta_{i,j}$. We use Lagrange polynomials as the basis functions. So for first degree basis functions, all mesh points $\mathbf{r}_t$ are vertices of triangles. Second degree basis functions require mesh points to be located at the vertices and on the side edges [19] [28].

Next, let $w(\mathbf{r}) = w_o(\mathbf{r})$ and $k(\mathbf{r}) = \frac{\partial w_o(\mathbf{r})}{\partial \mathbf{n}_o}$. Then, we can interpolate w and k using the Lagrange basis functions as follows:

$$
w(\mathbf{r}) \approx \sum_t w_t \psi_t(\mathbf{r}) = \sum_t w(\mathbf{r}_t)\psi_t(\mathbf{r}), \tag{49}
$$

$$
k(\mathbf{r}) \approx \sum_t k_t \psi_t(\mathbf{r}) = \sum_t k(\mathbf{r}_t)\psi_t(\mathbf{r}). \tag{50}
$$

Now, rewriting (36) and (48) in terms of the unknowns w_t and k_t, we have

$$
\begin{aligned}
w(\mathbf{p}) &- \sum_t k_t \oint_S \varepsilon_o \left(G_i(\mathbf{r},\mathbf{p}) - G_o(\mathbf{r},\mathbf{p})\right)\psi_t(\mathbf{r})\,\mathrm{d}S(\mathbf{r}) \\
&- \sum_t w_t \oint_S \left(\varepsilon_o \frac{\partial G_o(\mathbf{r},\mathbf{p})}{\partial \mathbf{n}_o} - \varepsilon_i \frac{\partial G_i(\mathbf{r},\mathbf{p})}{\partial \mathbf{n}_o}\right)\psi_t(\mathbf{r})\,\mathrm{d}S(\mathbf{r}) \\
&= \oint_S \left(\varepsilon_o G_i(\mathbf{r},\mathbf{p})\frac{\partial H(\mathbf{r},\mathbf{r}_s)}{\partial \mathbf{n}_o} - \varepsilon_i H(\mathbf{r},\mathbf{r}_s)\frac{G_i(\mathbf{r},\mathbf{p})}{\partial \mathbf{n}_o}\right)\mathrm{d}S(\mathbf{r}) \\
&+ \oint_S \left(\varepsilon_o G_i(\mathbf{r},\mathbf{p})\frac{\partial T(\mathbf{r},\mathbf{r}_s)}{\partial \mathbf{n}_o} - \varepsilon_i T(\mathbf{r},\mathbf{r}_s)\frac{G_i(\mathbf{r},\mathbf{p})}{\partial \mathbf{n}_o}\right)\mathrm{d}S(\mathbf{r}) \\
&- \frac{1}{2}H(\mathbf{p},\mathbf{r}_s) - \frac{1}{2}T(\mathbf{p},\mathbf{r}_s),
\end{aligned} \tag{51}
$$

$$
\begin{aligned}
\left(\frac{1}{2}+\frac{1}{2}\frac{\varepsilon_o}{\varepsilon_i}\right)k(\mathbf{p}) &- \sum_t w_t \oint\limits_S \left(\varepsilon_o \frac{\partial^2 G_o(\mathbf{r},\mathbf{p})}{\partial \mathbf{n}'_o \partial \mathbf{n}_o} - \varepsilon_i \frac{\partial^2 G_i(\mathbf{r},\mathbf{p})}{\partial \mathbf{n}'_o \partial \mathbf{n}_o}\right)\psi_t(\mathbf{r})\,\mathrm{d}S(\mathbf{r}) \\
&- \sum_t k_t \oint\limits_S \varepsilon_o \left(\frac{\partial G_i(\mathbf{r},\mathbf{p})}{\partial \mathbf{n}'_o} - \frac{\partial G_o(\mathbf{r},\mathbf{p})}{\partial \mathbf{n}'_o}\right)\psi_t(\mathbf{r})\,\mathrm{d}S(\mathbf{r}) \\
&= \oint\limits_S \varepsilon_o \frac{\partial G_i(\mathbf{r},\mathbf{p})}{\partial \mathbf{n}'_o}\left(\frac{\partial H(\mathbf{r},\mathbf{r}_s)}{\partial \mathbf{n}_o} + \frac{\partial T(\mathbf{r},\mathbf{r}_s)}{\partial \mathbf{n}_o}\right)\mathrm{d}S(\mathbf{r}) \\
&- \oint\limits_{S\setminus S_a} \varepsilon_i (H(\mathbf{r},\mathbf{r}_s)+T(\mathbf{r},\mathbf{r}_s))\frac{\partial^2 G_i(\mathbf{r},\mathbf{p})}{\partial \mathbf{n}'_o \partial \mathbf{n}_o}\,\mathrm{d}S(\mathbf{r}) \\
&+ \oint\limits_{S_a} \varepsilon_i (v(\mathbf{r})-H(\mathbf{r},\mathbf{r}_s)-T(\mathbf{r},\mathbf{r}_s))\frac{\partial^2 G_i(\mathbf{r},\mathbf{p})}{\partial \mathbf{n}'_o \partial \mathbf{n}_o}\,\mathrm{d}S(\mathbf{r}) \\
&+ \oint\limits_\Gamma \varepsilon_i v(\mathbf{r})\frac{\partial^2 G_i(\mathbf{r},\mathbf{p})}{\partial \mathbf{n}'_o \partial \mathbf{n}_\Gamma}\,\mathrm{d}S(\mathbf{r}) - \oint\limits_{S_a} \varepsilon_i \frac{\partial G_i(\mathbf{r},\mathbf{p})}{\partial \mathbf{n}'_o}\frac{\partial v(\mathbf{r})}{\partial \mathbf{n}_o}\,\mathrm{d}S(\mathbf{r}) \\
&- \oint\limits_\Gamma \varepsilon_i \frac{\partial G_i(\mathbf{r},\mathbf{p})}{\partial \mathbf{n}_o}\frac{\partial v(\mathbf{r})}{\partial \mathbf{n}_\Gamma}\,\mathrm{d}S(\mathbf{r}) + \frac{1}{2}\frac{\partial v(\mathbf{p})}{\partial \mathbf{n}_o} \\
&- \frac{1}{2}\frac{\varepsilon_o}{\varepsilon_i}\frac{\partial H(\mathbf{p},\mathbf{r}_s)}{\partial \mathbf{n}} - \frac{1}{2}\frac{\varepsilon_o}{\varepsilon_i}\frac{\partial T(\mathbf{p},\mathbf{r}_s)}{\partial \mathbf{n}}
\end{aligned}
\tag{52}
$$

For the sake of simplicity, let the following operators be defined.

(53)

$$
\begin{aligned}
S0 &= \oint\limits_S G_i(\mathbf{r},\mathbf{p})\psi_t(\mathbf{r})\,\mathrm{d}S(\mathbf{r}), & S1 &= \oint\limits_S G_o(\mathbf{r},\mathbf{p})\psi(\mathbf{r})\,\mathrm{d}S(\mathbf{r}), \\
D0 &= \oint\limits_S \tfrac{\partial G_i(\mathbf{r},\mathbf{p})}{\partial \mathbf{n}_o}\psi_t(\mathbf{r})\,\mathrm{d}S(\mathbf{r}), & D1 &= \oint\limits_S \tfrac{\partial G_o(\mathbf{r},\mathbf{p})}{\partial \mathbf{n}_o}\psi_t(\mathbf{r})\,\mathrm{d}S(\mathbf{r}), \\
D2 &= \oint\limits_S \tfrac{\partial G_i(\mathbf{r},\mathbf{p})}{\partial \mathbf{n}'_o}\psi_t(\mathbf{r})\,\mathrm{d}S(\mathbf{r}), & D3 &= \oint\limits_S \tfrac{\partial G_o(\mathbf{r},\mathbf{p})}{\partial \mathbf{n}'_o}\psi_t(\mathbf{r})\,\mathrm{d}S(\mathbf{r}), \\
T0 &= \oint\limits_S \tfrac{\partial^2 G_i(\mathbf{r},\mathbf{p})}{\partial \mathbf{n}'_o \partial \mathbf{n}_o}\psi_t(\mathbf{r})\,\mathrm{d}S(\mathbf{r}), & T1 &= \oint\limits_S \tfrac{\partial^2 G_o(\mathbf{r},\mathbf{p})}{\partial \mathbf{n}'_o \partial \mathbf{n}_o}\psi_t(\mathbf{r})\,\mathrm{d}S(\mathbf{r}), \\
J5 &= -\oint\limits_\Gamma \varepsilon_i \left(\tfrac{\partial G_i(\mathbf{r},\mathbf{p})}{\partial \mathbf{n}'_o}\tfrac{\partial v(\mathbf{r})}{\partial \mathbf{n}_\Gamma}\right)\mathrm{d}S(\mathbf{r}), & J6 &= -\oint\limits_{S_a} \varepsilon_i \left(\tfrac{\partial G_i(\mathbf{r},\mathbf{p})}{\partial \mathbf{n}'_o}\tfrac{\partial v(\mathbf{r})}{\partial \mathbf{n}_o}\right)\mathrm{d}S(\mathbf{r}), \\
J7 &= \oint\limits_\Gamma \varepsilon_i \left(v(\mathbf{r})\tfrac{\partial^2 G_i(\mathbf{r},\mathbf{p})}{\partial \mathbf{n}'_o \partial \mathbf{n}_\Gamma}\right)\mathrm{d}S(\mathbf{r}), & L0 &= \tfrac{1}{2}\tfrac{\partial v_o(\mathbf{p})}{\partial \mathbf{n}_o}, \\
L1 &= -\tfrac{1}{2}H(\mathbf{p},\mathbf{r}_s), & L2 &= -\tfrac{1}{2}T(\mathbf{p},\mathbf{r}_s), \\
L3 &= -\tfrac{1}{2}\tfrac{\varepsilon_o}{\varepsilon_i}\tfrac{\partial H(\mathbf{p},\mathbf{r}_k)}{\partial \mathbf{n}_o}, & L4 &= -\tfrac{1}{2}\tfrac{\varepsilon_o}{\varepsilon_i}\tfrac{\partial T(\mathbf{p},\mathbf{r}_k)}{\partial \mathbf{n}_o},
\end{aligned}
$$

and

$$
J0 = \oint\limits_S \left(\varepsilon_o G_i(\mathbf{r},\mathbf{p})\frac{\partial H(\mathbf{r},\mathbf{r}_s)}{\partial \mathbf{n}_o} - \varepsilon_i H(\mathbf{r},\mathbf{r}_s)\frac{\partial G_i(\mathbf{r},\mathbf{p})}{\partial \mathbf{n}_o}\right)\mathrm{d}S(\mathbf{r}), \tag{54}
$$

$$J1 = \oint_S \left(\varepsilon_o G_i(\mathbf{r},\mathbf{p}) \frac{\partial T(\mathbf{r},\mathbf{r}_s)}{\partial \mathbf{n}_o} - \varepsilon_i T(\mathbf{r},\mathbf{r}_s) \frac{\partial G_i(\mathbf{r},\mathbf{p})}{\partial \mathbf{n}_o} \right) \mathrm{d}S(\mathbf{r}), \tag{55}$$

$$J2 = \oint_{S_a} \varepsilon_i (v(\mathbf{r}) - H(\mathbf{r},\mathbf{r}_s) - T(\mathbf{r},\mathbf{r}_s)) \frac{\partial^2 G_i(\mathbf{r},\mathbf{p})}{\partial \mathbf{n}_o' \partial \mathbf{n}_o} \mathrm{d}S(\mathbf{r}), \tag{56}$$

$$J3 = \oint_S \varepsilon_o \frac{\partial G_i(\mathbf{r},\mathbf{p})}{\partial \mathbf{n}_o'} \left(\frac{\partial H(\mathbf{r},\mathbf{r}_s)}{\partial \mathbf{n}_o} + \frac{\partial T(\mathbf{r},\mathbf{r}_s)}{\partial \mathbf{n}_o} \right) \mathrm{d}S(\mathbf{r}), \tag{57}$$

$$J4 = -\oint_S \oint_{S_a} \varepsilon_i (H(\mathbf{r},\mathbf{r}_s) + T(\mathbf{r},\mathbf{r}_s)) \frac{\partial^2 G_i(\mathbf{r},\mathbf{p})}{\partial \mathbf{n}_o' \partial \mathbf{n}_o} \mathrm{d}S(\mathbf{r}). \tag{58}$$

Then we can rewrite (36) and (48) as the following matrix equation:

$$\left[\begin{pmatrix} I & 0 \\ 0 & \left(\frac{1}{2} + \frac{1}{2}\frac{\varepsilon_o}{\varepsilon_i}\right) I \end{pmatrix} + \begin{pmatrix} (\varepsilon_i D0 - \varepsilon_o D1) & -(S0 - S1)\,\varepsilon_o \\ (\varepsilon_i T0 - \varepsilon_o T1) & -(D2 - D3)\,\varepsilon_o \end{pmatrix} \right] \begin{pmatrix} w_o \\ k_o \end{pmatrix} = \begin{pmatrix} J0 + J1 + L1 + L2 \\ J2 + J3 + J4 + J5 + J6 + J7 + L0 + L3 + L4 \end{pmatrix}, \tag{59}$$

where $\mathbf{p}$ takes different mesh points $\mathbf{r}_t$ in different rows of the matrix.

The overall goal of introducing the subtraction $w_o = \phi_o - H - T$ becomes more visible: the matrix equation solves for smoother variable w_o and its derivative, while the right-hand side vector $\mathbf{b}$ contains the part of the potential that is more difficult to calculate, H and T. That implies that emphasis shifts to calculating these auxiliary integrals accurately so that the matrix solver produces accurate results for w_o and its derivative.

5.2. Calculation of right-hand-side integrals in (59)

5.2.1. Computing integral over S_a Various integrals on the right hand side of (59) need to be calculated accurately over the interior hemisphere Γ at each mesh point location $\mathbf{p}$, over the patch S_a, or over the sphere S or $S \backslash S_a$. Mapped tensor product Gauss quadrature is used. As the region S_a is a circular region on the spheroid whose boundary in general is not a constant θ line, the bounds of integration are difficult to handle in terms of the polar and azimuthal angles of the sphere. Secondly, even if we could easily find the bounds of integration that determines region S_a, there is a possibility that one of the Gauss points (ϕ_i, θ_j) accidentally has the same location as point $\mathbf{p}$. This would introduce a singularity in the integrand, making calculation impossible.

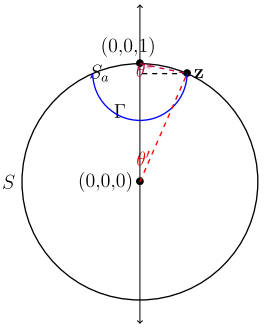

Figure 3: Finding necessary angles when integrating over surface of sphere.

We address these two issues by introducing a reference sphere, as shown in Figure 3. The north pole is taken to be the location of the mesh point $\mathbf{p}$, and we have a hemisphere of radius a centered at $\mathbf{p}$. There are two angles that are important, labeled θ^* and θ'.

For different integral terms in the right hand side of (59), we choose appropriate bounds under the assumption that the mesh point is located at the north pole of the large sphere. So for example, for integral over S_a, the Gauss points are distributed over $[0, \theta'] \times [0, 2\pi]$, and for an integral over Γ, over $[\theta^*, \pi] \times [0, 2\pi]$.

The rotation required to map reference point $\mathbf{p}'$, located at the the north pole of the reference sphere, to the arbitrary point $\mathbf{p}$ is given by

$$(x_t, y_t, z_t) = R_z(-\alpha) * R_x(-\gamma) * (x, y, z)^T, \tag{60}$$

where

$$R_x(\gamma) = \begin{bmatrix} 1 & 0 & 0 \\ 0 & \cos(\gamma) & -\sin(\gamma) \\ 0 & \sin(\gamma) & \cos(\gamma) \end{bmatrix} \quad \text{and} \quad R_z(\alpha) = \begin{bmatrix} \cos(\alpha) & -\sin(\alpha) & 0 \\ \sin(\alpha) & \cos(\alpha) & 0 \\ 0 & 0 & 1 \end{bmatrix}. \tag{61}$$

Then boundary integrals, centered at arbitrary mesh location point $\mathbf{p}$, are now evaluated as follows:

$$\oint f(x, y, z)\, \mathrm{d}x\, \mathrm{d}y\, \mathrm{d}z \approx \sum_{i=1}^{M} \sum_{j=1}^{N} w_i \hat{w}_j f(x_t, y_t, z_t) r^2 \sin(\theta_j), \tag{62}$$

where the bounds of integration for the rotated integrals are the same as in the integrals of the un-rotated reference sphere.

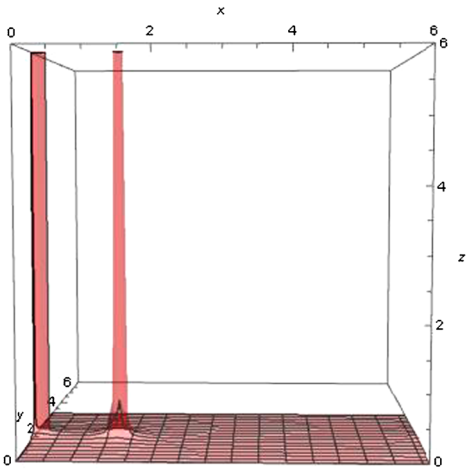

Figure 4: Graph of the integrand J0 for mesh point $\mathbf{p} = (1, 0, 0)$ and source $\mathbf{r}_s = (0.2438, 0.9752, 0.0975)$, which is 0.01 units away from the surface of the sphere.

5.2.2. Adaptive quadratures for singular right-hand-side integrals In subtracting the $H(\mathbf{r}, \mathbf{r}_s)$ and $T(\mathbf{r}, \mathbf{r}_s)$ functions from the electric potential and re-deriving the boundary integral equations in terms of $w_o = \phi - H - T$, we shift the most difficult-to-calculate parts of the potential to the right-hand side auxiliary integrals in the BIEs and resulting matrix equation (59). Therefore, to get accurate results for the potential, we must be able to calculate those right-hand side integrals extremely accurately. In the case of the examples of the last section, this meant using millions Gauss points with a naive approach on some integrals in order to achieve sufficient accuracy to result in those small relative errors. While this does indeed yield the desired effect, it is computationally expensive and rather wasteful, as such densities of Gauss points on the integrals are only necessary in specific locations. So in this section, we use adaptive quadratures to reduce the amount of Gauss points required to calculate the auxiliary integrals accurately, while maintaining the accuracy in the potentials. This makes the subtraction technique in the boundary integral equations more efficient.

To begin this process, we observe that singular behavior in the auxiliary integrals $J0 - J7$ is displayed in two regions: around each mesh point location $\mathbf{p}$ and around the projection of the source charge on the sphere $\mathbf{r}'_s$. For instance, Figures 4, 5 shows the graph of the integrand $J0$ where the two "spikes" around those two regions show singular behavior. In order to

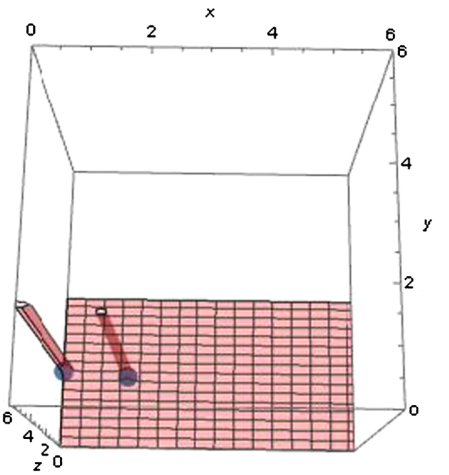

Figure 5: Top view of the same graph, with balls indicating where $\mathbf{p}$ and $\mathbf{r}_s$ are.

capture all of that singularity and calculate those integrals accurately, more Gauss points should be placed around these two locations.

- Subdomain grid

We partition the integration domain into subdomains, only putting a dense coverage of points where needed, and then fewer points elsewhere; the resulting calculation technique being an adaptive integration quadrature. Initially, each of our RHS integrals are calculated as written above in (62), written again here for convenience:

$$\oint f(x,y,z)\,\mathrm{d}x\,\mathrm{d}y\,\mathrm{d}z \approx \sum_{i=1}^{M}\sum_{j=1}^{N} w_i \hat{w}_j f(x_t, y_t, z_t) r^2 \sin(\theta_j). \tag{63}$$

For each integral, the Gauss points and weights are calculated to be spread over a set of bounds that would cover the entirety of whatever boundary region the integrals dictated. So for example for integral $J0$, which is defined over the entire spherical surface area S, the Gauss points would be distributed over the region $[0,\pi]\times[0,2\pi]$.

However, to better allocate Gauss points where needed, we start by taking a standard region that an integral is calculated over, $\theta_{min} \le \theta \le \theta_{max}$ and $\phi_{min} \le \phi \le \phi_{max}$, and subdividing this region into blocks of smaller sizes. This creates a grid pattern seen in Figure 6. For each subdivision or "box", we use the scaled tensor product Gauss-Legendre quadrature formula.

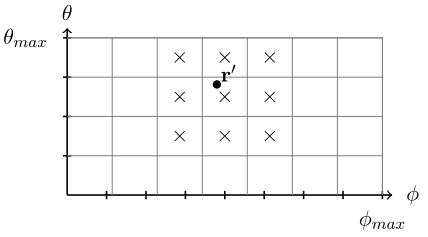

Figure 6: Boxes that have a dense distribution of Gauss points around **p**.

Now for an arbitrary m, n-box, we can distribute a higher number of Gauss points in that specific box, while leaving other boxes with a much lower density.

- Quadrature point distributions

We have previously shown that we need more Gauss points in the region around mesh point **p** and the projection of the source $\mathbf{r}_s$ onto the sphere. So we want to identify into which m, n boxes these two points on the surface of the sphere fall. For this, we determine what the respective (ϕ', θ') coordinates of these points are and find which m, n makes the following test true:

$$mI_\theta \leq \theta' \leq (m+1)I_\theta$$
$$nI_\phi \leq \phi' \leq (n+1)I_\phi.$$

Knowing into which m, n box the point falls, we assign an increased number of points to that box, the density of which can vary, depending.

In the event that a point of interest $\mathbf{r}'$ does not fall directly into the center of the m, n-box, which happens more often than not, not all of the singular region of the integrand around that point is entirely contained in that box. To eliminate this issue, we dictate that all of m, n-box's neighbors have denser points as well, as shown by the ×'d boxes in Figure 6. This creates a region large enough to capture all of the integrand's singularity, regardless of where the point is located in the m, n-box. When the divisions size, p and q, are sufficiently large (but not too large, as the boxes become too small to capture all behavior), then we have a significant portion of the rest of the boundary where we can distribute fewer points, as there is no singular behavior there.

This now gives us the perfect setup by which we can place more Gauss points around mesh point **p** *and* the source projection location $\mathbf{r}'_s$. Using this grid system in Figure 6, we ensure that a circular region of denser Gauss points is allocated around mesh point **p** by dictating that the top row of boxes

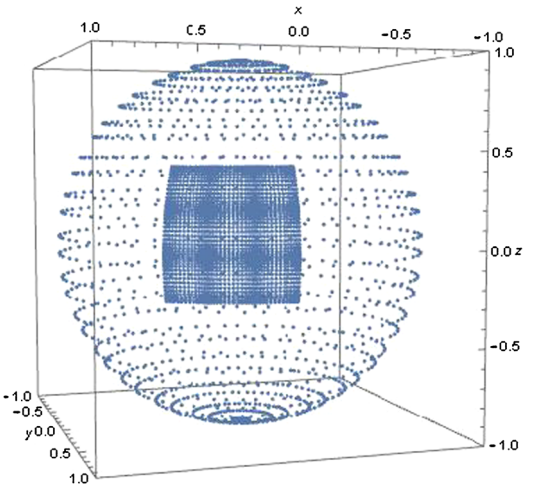

Figure 7: The nine boxes with a denser Gauss pt distribution visible.

in the grid all have denser coverage. To then take care of the second region $\mathbf{r}'_s$ where denser points are needed, we use the nine-box rectangular patch shown in Figure 7. This results in a Gauss point distribution with two dense patches being used simultaneously in order to capture all singular behavior of the integrands around those two locations.

We should note here that simply using polar coordinates to only allocate more Gauss points around the mesh point $\mathbf{p}$ was insufficient to generate the desired calculation accuracy in evaluating the integrals. The singular behavior around the source projection point $\mathbf{r}'_s$ must be addressed as well, especially once the source gets extremely close to the sphere's surface, thus making this two-patch quadrature approach necessary.

6. Integral equations for a system of dielectric spheres

In this section, we extend the subtraction technique and provide an updated set of boundary integral equations for a system of more than one sphere interacting with a source charge.

First, we discuss our subtraction technique regarding the use of the image subtraction function $T(\mathbf{r}, \mathbf{r}_s)$ for a system of dielectric spheres. Whether discussing the boundary integral equations of one sphere or a system of them, we always have the choice to set $T(\mathbf{r}, \mathbf{r}_s) = 0$, and the integral equations are still true and easily usable. Recall that $T(\mathbf{r}, \mathbf{r}_s)$ represents the first few terms of an image approximation of the reaction field ϕ_{rf} of the potential ϕ [8]. In

setting $T(\mathbf{r}, \mathbf{r}_s)$ equal to the first few terms in this approximation and including it in the subtraction $w_o(\mathbf{r}) = \phi(\mathbf{r}) - H(\mathbf{r}, \mathbf{r}_s) - T(\mathbf{r}, \mathbf{r}_s)$, we increase the accuracy in approximating ϕ, specifically for the case when a source charge $\mathbf{r}_s$ is very close to the surface of the sphere(s). When $\mathbf{r}_s$ is not close enough to cause singular behavior in the integrands in the BIE's, the function $T(\mathbf{r}, \mathbf{r}_s)$ is unnecessary to obtain good accuracy.

We incorporate the option to use $T(\mathbf{r}, \mathbf{r}_s)$ on sphere S_j if it is within a tolerance distance δ to the source $\mathbf{r}_s$. If the minimum distance of the sphere to the source is greater than δ, we set $T(\mathbf{r}, \mathbf{r}_s) = 0$ on that sphere, as $T(\mathbf{r}, \mathbf{r}_s)$ is not needed.

Let j and k be differing indexes for functions $w_o(\mathbf{r})$ and $T(\mathbf{r}, \mathbf{r}_s)$ defined on spheres j and k, and let $\delta > 0$ be a tolerance value for the minimum distance between the surface of any particular sphere S_k in the system and a source charge $\mathbf{r}_s$. We dictate that if $\min(||S_k - \mathbf{r}_s||) < \delta$ for sphere S_k, then we use the function $T_k(\mathbf{r}, \mathbf{r}_s)$ to estimate the reaction field on that specific sphere k.

Now to adapt the BIEs to multiple-sphere interactions, we redefine the function $T(\mathbf{r}, \mathbf{r}_s)$ to be equal to the sum of the T terms over the L total spheres where the function is needed. That is,

$$T(\mathbf{r}, \mathbf{r}_s) = T_1(\mathbf{r}, \mathbf{r}_s) + T_2(\mathbf{r}, \mathbf{r}_s) + \cdots, \quad l = 1, \cdots, L. \tag{64}$$

So then

$$w_k(\mathbf{r}) = \begin{cases} \phi_o(\mathbf{r}) - H(\mathbf{r}, \mathbf{r}_s) - T(\mathbf{r}, \mathbf{r}_s) & \mathbf{r} \in \Omega_{o_k}, \\ \phi_i(\mathbf{r}) & \mathbf{r} \in \Omega_{i_k}, \end{cases} . \tag{65}$$

Let $0 < j \leq J$ for J total spheres in the system, and let $0 < k \leq J$, where k is not necessarily the same as j. Then the first boundary integral equation of the first kind is

$$\frac{1}{2} w_{o_k}(\mathbf{p}) = \sum_{j=1}^{J} \int_{S_j} \varepsilon_o(\mathbf{r}) \left(w_{o_k}(\mathbf{r}) \frac{\partial G_o(\mathbf{r}, \mathbf{p})}{\partial \mathbf{n}} - G_o(\mathbf{r}, \mathbf{p}) \frac{\partial w_{o_k}(\mathbf{r})}{\partial \mathbf{n}} \right) \mathrm{d}S(\mathbf{r}) \tag{66}$$

and the second integral equation of the first kind is

$$\begin{aligned} &\frac{1}{2} w_{o_k}(\mathbf{p}) - \sum_{j=1}^{J} \int_{S_j} \left(\varepsilon_o(\mathbf{r}) G_i(\mathbf{r}, \mathbf{p}) \frac{\partial w_{o_j}(\mathbf{r})}{\partial \mathbf{n}} - \varepsilon_o(\mathbf{r}) w_{o_j}(\mathbf{r}) \frac{\partial G_i(\mathbf{r}, \mathbf{p})}{\partial \mathbf{n}} \right) \mathrm{d}S(\mathbf{r}) \\ &= \sum_{j=1}^{J} \int_{S_j} \left(\varepsilon_o(\mathbf{r}) G_i(\mathbf{r}, \mathbf{p}) \frac{\partial H(\mathbf{r}, \mathbf{r}_s)}{\partial \mathbf{n}} - \varepsilon_i(\mathbf{r}) H(\mathbf{r}, \mathbf{r}_s) \frac{\partial G_i(\mathbf{r}, \mathbf{p})}{\partial \mathbf{n}} \right) \mathrm{d}S(\mathbf{r}) \end{aligned}$$

$$+\sum_{j=1}^{J}\int_{S_j}\left(\varepsilon_o(\mathbf{r})G_i(\mathbf{r},\mathbf{p})\frac{\partial T(\mathbf{r},\mathbf{r}_s)}{\partial \mathbf{n}}-\varepsilon_i(\mathbf{r})T(\mathbf{r},\mathbf{r}_s)\frac{\partial G_i(\mathbf{r},\mathbf{p})}{\partial \mathbf{n}}\right)\mathrm{d}S(\mathbf{r})$$

$$-\frac{1}{2}H(\mathbf{r},\mathbf{r}_s)-\frac{1}{2}T(\mathbf{r},\mathbf{r}_s) \tag{67}$$

To develop the integral equations of the second kind, we need to take the normal derivatives of the two previous integral equations. The derivative of (66), after taking the limit of $\mathbf{r}$ to the surface of the spheres, is

$$\frac{1}{2}\frac{w_{o_k}(\mathbf{r})}{\partial \mathbf{n}_k}=\sum_{j=1}^{J}\int_{S_j}\varepsilon_o(\mathbf{r})\left(w_{o_j}(\mathbf{r})\frac{\partial^2 G_o(\mathbf{r},\mathbf{p})}{\partial \mathbf{n}'\partial \mathbf{n}}-\frac{\partial G_o(\mathbf{r},\mathbf{p})}{\partial \mathbf{n}'}\frac{w_{o_j}(\mathbf{r})}{\partial \mathbf{n}}\right)\mathrm{d}S(\mathbf{r}) \tag{68}$$

and the derivative of the (67), after taking the limit of $\mathbf{r}$ to the surface of the spheres, is

$$\begin{aligned}
&\frac{1}{2}\frac{\varepsilon_o(\mathbf{r})}{\varepsilon_i(\mathbf{r})}\frac{\partial w_{o_k}(\mathbf{p})}{\partial \mathbf{n}_k}\\
&-\sum_{j=1}^{J}\int_{S_j}\left(\varepsilon_o(\mathbf{r})\frac{\partial G_i(\mathbf{r},\mathbf{p})}{\partial \mathbf{n}'}\frac{\partial w_{o_j}(\mathbf{r})}{\partial \mathbf{n}}-\varepsilon_i(\mathbf{r})w_{o_j}(\mathbf{r})\frac{\partial^2 G_i(\mathbf{r},\mathbf{p})}{\partial \mathbf{n}'\partial \mathbf{n}}\right)\mathrm{d}S(\mathbf{r})\\
&=\sum_{j=1}^{J}\int_{S_j}\left(\varepsilon_o(\mathbf{r})\frac{\partial G_i(\mathbf{r},\mathbf{p})}{\partial \mathbf{n}'}\frac{\partial H(\mathbf{r},\mathbf{r}_s)}{\partial \mathbf{n}}-\varepsilon_i(\mathbf{r})H(\mathbf{r},\mathbf{r}_s)\frac{\partial^2 G_i(\mathbf{r},\mathbf{p})}{\partial \mathbf{n}'\partial \mathbf{n}}\right)\mathrm{d}S(\mathbf{r})\\
&+\sum_{j=1}^{J}\int_{S_j}\left(\varepsilon_o(\mathbf{r})\frac{\partial G_i(\mathbf{r},\mathbf{p})}{\partial \mathbf{n}'}\frac{\partial T(\mathbf{r},\mathbf{r}_s)}{\partial \mathbf{n}}-\varepsilon_i(\mathbf{r})T(\mathbf{r},\mathbf{r}_s)\frac{\partial^2 G_i(\mathbf{r},\mathbf{p})}{\partial \mathbf{n}'\partial \mathbf{n}}\right)\mathrm{d}S(\mathbf{r})\\
&-\frac{1}{2}\frac{\varepsilon_o(\mathbf{r})}{\varepsilon_i(\mathbf{r})}\frac{\partial H(\mathbf{p},\mathbf{r}_s)}{\partial \mathbf{n}_k}-\frac{1}{2}\frac{\varepsilon_o(\mathbf{r})}{\varepsilon_i(\mathbf{r})}\frac{\partial T(\mathbf{p},\mathbf{r}_s)}{\partial \mathbf{n}_k}.
\end{aligned} \tag{69}$$

Adding the two equations of the first kind, (66) and (67), gives the first integral equation of the second kind, and adding the derivatives of the two first kind equations, (68) and (69), gives the second equation of the second kind.

$$\begin{aligned}
&w_{o_k}(\mathbf{p})-\sum_{j=1}^{J}\int_{S_j}\varepsilon_o(\mathbf{r})\left(G_i(\mathbf{r},\mathbf{p})-G_o(\mathbf{r},\mathbf{r}_s)\right)\frac{\partial w_{o_j}(\mathbf{r})}{\partial \mathbf{n}_o}\mathrm{d}S(\mathbf{r})\\
&=\sum_{j=1}^{J}\int_{S_j}\left(\varepsilon_o(\mathbf{r})G_i(\mathbf{r},\mathbf{p})\frac{\partial H(\mathbf{r},\mathbf{r}_s)}{\partial \mathbf{n}_o}-\varepsilon_i(\mathbf{r})H(\mathbf{r},\mathbf{r}_s)\frac{\partial G_i(\mathbf{r},\mathbf{p})}{\partial \mathbf{n}_o}\right)\mathrm{d}S(\mathbf{r})
\end{aligned}$$

$$+\sum_{j=1}^{J}\int_{S_j}\left(\varepsilon_o(\mathbf{r})G_i(\mathbf{r},\mathbf{p})\frac{\partial T(\mathbf{r},\mathbf{r}_s)}{\partial \mathbf{n}_o}-\varepsilon_i(\mathbf{r})T(\mathbf{r},\mathbf{r}_s)\frac{\partial G_i(\mathbf{r},\mathbf{p})}{\partial \mathbf{n}_o}\right)\mathrm{d}S(\mathbf{r})$$

$$-\frac{1}{2}H(\mathbf{r},\mathbf{r}_s)-\frac{1}{2}T(\mathbf{r},\mathbf{r}_s) \tag{70}$$

and

$$\begin{aligned}
&\left(\frac{1}{2}+\frac{1}{2}\frac{\varepsilon_o(\mathbf{r})}{\varepsilon_i(\mathbf{r})}\right)\frac{\partial w_{o_k}(\mathbf{p})}{\partial \mathbf{n}_{o_k}}\\
&-\sum_{j=1}^{J}\int_{S_j}\left(\varepsilon_o(\mathbf{r})\frac{\partial^2 G_o(\mathbf{r},\mathbf{p})}{\partial \mathbf{n}_o'\partial \mathbf{n}_o}-\varepsilon_i(\mathbf{r})\frac{\partial^2 G_i(\mathbf{r},\mathbf{p})}{\partial \mathbf{n}_o'\partial \mathbf{n}_o}\right)w_{o_j}(\mathbf{r})\,\mathrm{d}S(\mathbf{r})\\
&-\sum_{j=1}^{J}\int_{S_j}\left(\varepsilon_o(\mathbf{r})\frac{\partial G_i(\mathbf{r},\mathbf{p})}{\partial \mathbf{n}_o'}-\varepsilon_o(\mathbf{r})\frac{\partial G_o(\mathbf{r},\mathbf{p})}{\partial \mathbf{n}_o'}\right)\frac{\partial w_{o_j}(\mathbf{r})}{\partial \mathbf{n}_o}\,\mathrm{d}S(\mathbf{r})\\
&-\sum_{j=1}^{J}\text{p.f.}\int_{S_j}\varepsilon_i(\mathbf{r})\left(H(\mathbf{r},\mathbf{r}_s)+T(\mathbf{r},\mathbf{r}_s)\right)\frac{\partial^2 G_i(\mathbf{r},\mathbf{p})}{\partial \mathbf{n}_o'\partial \mathbf{n}_o}\,\mathrm{d}S(\mathbf{r})\\
&+\sum_{j=1}^{J}\int_{S_j}\varepsilon_o(\mathbf{r})\left(\frac{\partial H(\mathbf{r},\mathbf{r}_s)}{\partial \mathbf{n}_o}+\frac{\partial T(\mathbf{r},\mathbf{r}_s)}{\partial \mathbf{n}_o}\right)\frac{\partial G_i(\mathbf{r},\mathbf{p})}{\partial \mathbf{n}_o'}\,\mathrm{d}S(\mathbf{r})\\
&-\frac{1}{2}\frac{\varepsilon_o(\mathbf{r})}{\varepsilon_i(\mathbf{r})}\frac{\partial H(\mathbf{r},\mathbf{r}_s)}{\partial \mathbf{n}_{o_k}}-\frac{1}{2}\frac{\varepsilon_o(\mathbf{r})}{\varepsilon_i(\mathbf{r})}\frac{\partial T(\mathbf{r},\mathbf{r}_s)}{\partial \mathbf{n}_{o_k}}
\end{aligned} \tag{71}$$

Before going further, we should note that equation (71) does not yet include the use of the "bubble technique" we developed to regularize the finite part integrals. In addition, we have the option to pick and choose when and on which sphere(s) the bubble method and image subtraction method are used. As a reminder, the so-called "bubble technique" is used to regularize the following integral:

$$\xi=-\text{p.f.}\oint_S\varepsilon_i(H(\mathbf{r},\mathbf{r}_s)+T(\mathbf{r},\mathbf{r}_s))\frac{\partial^2 G_i(\mathbf{r},\mathbf{p})}{\partial \mathbf{n}'\partial \mathbf{n}}\,\mathrm{d}S(\mathbf{r}). \tag{72}$$

Its integrand is hypersingular, and therefore difficult to accurately calculate, when mesh point $\mathbf{p}$ is close to watch point $\mathbf{r}$. This difficulty is mitigated by using the identity (44), which distributes the computational load over a more manageable set of integrals. As a result, for the integral equations of one sphere, this identity is used for every row in the matrix equation (59).

However, when discussing the boundary integral equations of a *system* of spheres, this integral is calculated J times. This means that any given mesh point $\mathbf{p}$ is not located on every sphere S_j being integrated over in the sum of J finite part integrals, but $\mathbf{p}$ is always on *one* of them. In the case where $\mathbf{p}$ and $\mathbf{r}$ are located on different spheres for the integral ξ_j, the second derivative of the Green's function in ξ does not display singular behavior, and therefore the subsequent exchange of integrals through the identity (44) is not necessary. So we then only use the identity (44) for the particular integral ξ_j in the sum that corresponds to the same sphere on which $\mathbf{p}$ is located, but not the other integrals in the sum. Incorporating this idea into (71), it is now modified to be:

$$
\begin{aligned}
&\left(\frac{1}{2}+\frac{1}{2}\frac{\varepsilon_o(\mathbf{r})}{\varepsilon_i(\mathbf{r})}\right)\frac{\partial w_{o_k}(\mathbf{p})}{\partial \mathbf{n}_{o_k}}\\
&-\sum_{j=1}^{J}\int\limits_{S_j}\left(\varepsilon_o(\mathbf{r})\frac{\partial^2 G_o(\mathbf{r},\mathbf{p})}{\partial \mathbf{n}'_o\partial \mathbf{n}_o}-\varepsilon_i(\mathbf{r})\frac{\partial^2 G_i(\mathbf{r},\mathbf{p})}{\partial \mathbf{n}'_o\partial \mathbf{n}_o}\right)w_{o_j}(\mathbf{r})\,\mathrm{d}S(\mathbf{r})\\
&=\sum_{j=1}^{J}\int\limits_{S_j}\left(\varepsilon_o(\mathbf{r})\frac{\partial G_i(\mathbf{r},\mathbf{p})}{\partial \mathbf{n}'_o}-\varepsilon_o(\mathbf{r})\frac{\partial G_o(\mathbf{r},\mathbf{p})}{\partial \mathbf{n}'_o}\right)\frac{\partial w_{o_j}(\mathbf{r})}{\partial \mathbf{n}_o}\,\mathrm{d}S(\mathbf{r})\\
&-\sum_{j=1}^{J}\mathrm{p.f.}\int\limits_{S_j}\varepsilon_i(\mathbf{r})\left(H(\mathbf{r},\mathbf{r}_s)+T(\mathbf{r},\mathbf{r}_s)\right)\frac{\partial^2 G_i(\mathbf{r},\mathbf{p})}{\partial \mathbf{n}'_o\partial \mathbf{n}_o}\,\mathrm{d}S(\mathbf{r})\\
&+\sum_{j=1}^{J}\int\limits_{S_j}\varepsilon_o(\mathbf{r})\left(\frac{\partial H(\mathbf{r},\mathbf{r}_s)}{\partial \mathbf{n}_o}+\frac{\partial T(\mathbf{r},\mathbf{r}_s)}{\partial \mathbf{n}_o}\right)\frac{\partial G_i(\mathbf{r},\mathbf{p})}{\partial \mathbf{n}'_o}\,\mathrm{d}S(\mathbf{r})\\
&-\int\limits_{S_k\setminus S_{a_k}}\varepsilon_i(\mathbf{r})\left(H(\mathbf{r},\mathbf{r}_s)+T(\mathbf{r},\mathbf{r}_s)\right)\frac{\partial^2 G_i(\mathbf{r},\mathbf{p})}{\partial \mathbf{n}'_o\partial \mathbf{n}_o}\,\mathrm{d}S(\mathbf{r})\\
&+\int\limits_{S_{a_k}}\varepsilon_i(\mathbf{r})\left(v(\mathbf{r})-H(\mathbf{r},\mathbf{r}_s)-T(\mathbf{r},\mathbf{r}_s)\right)\frac{\partial^2 G_i(\mathbf{r},\mathbf{r}_s)}{\partial \mathbf{n}'_o\partial \mathbf{n}_o}\,\mathrm{d}S(\mathbf{r})\\
&-\int\limits_{S_{a_k}}\varepsilon_i(\mathbf{r})\frac{\partial G_i(\mathbf{r},\mathbf{p})}{\partial \mathbf{n}'_o}\frac{\partial v(\mathbf{r})}{\partial \mathbf{n}_o}\,\mathrm{d}S(\mathbf{r})\\
&-\int\limits_{\Gamma_k}\varepsilon_i(\mathbf{r})\frac{\partial G_i(\mathbf{r},\mathbf{p})}{\partial \mathbf{n}'_o}\frac{\partial v(\mathbf{r})}{\partial \mathbf{n}_\Gamma}\,\mathrm{d}S(\mathbf{r})+\int\limits_{\Gamma_k}\varepsilon_i(\mathbf{r})v(\mathbf{r})\frac{\partial^2 G_i(\mathbf{r},\mathbf{p})}{\partial \mathbf{n}'_o\partial \mathbf{n}_\Gamma}\,\mathrm{d}S(\mathbf{r})\\
&-\frac{1}{2}\frac{\varepsilon_o(\mathbf{r})}{\varepsilon_i(\mathbf{r})}\frac{\partial H(\mathbf{r},\mathbf{r}_s)}{\partial \mathbf{n}_{o_k}}-\frac{1}{2}\frac{\varepsilon_o(\mathbf{r})}{\varepsilon_i(\mathbf{r})}\frac{\partial T(\mathbf{r},\mathbf{r}_s)}{\partial \mathbf{n}_{o_k}}+\frac{1}{2}\frac{\partial v(\mathbf{p})}{\partial \mathbf{n}_{o_k}}.
\end{aligned}
\tag{73}
$$

We introduce the following integral operators

$$\begin{aligned} S0 &= \oint_S G_i(\mathbf{r},\mathbf{p})\psi_t(\mathbf{r})\,\mathrm{d}S(\mathbf{r}) & S1 &= \oint_S G_o(\mathbf{r},\mathbf{p})\psi(\mathbf{r})\,\mathrm{d}S(\mathbf{r}) \\ D0 &= \oint_S \tfrac{\partial G_i(\mathbf{r},\mathbf{p})}{\partial \mathbf{n}_o}\psi_t(\mathbf{r})\,\mathrm{d}S(\mathbf{r}) & D1 &= \oint_S \tfrac{\partial G_o(\mathbf{r},\mathbf{p})}{\partial \mathbf{n}_o}\psi_t(\mathbf{r})\,\mathrm{d}S(\mathbf{r}) \\ D2 &= \oint_S \tfrac{\partial G_i(\mathbf{r},\mathbf{p})}{\partial \mathbf{n}'_o}\psi_t(\mathbf{r})\,\mathrm{d}S(\mathbf{r}) & D3 &= \oint_S \tfrac{\partial G_o(\mathbf{r},\mathbf{p})}{\partial \mathbf{n}'_o}\psi_t(\mathbf{r})\,\mathrm{d}S(\mathbf{r}) \\ T0 &= \oint_S \tfrac{\partial^2 G_i(\mathbf{r},\mathbf{p})}{\partial \mathbf{n}'_o \partial \mathbf{n}_o}\psi_t(\mathbf{r})\,\mathrm{d}S(\mathbf{r}) & T1 &= \oint_S \tfrac{\partial^2 G_o(\mathbf{r},\mathbf{p})}{\partial \mathbf{n}'_o \partial \mathbf{n}_o}\psi_t(\mathbf{r})\,\mathrm{d}S(\mathbf{r}) \end{aligned}$$

and equations (70) (73) are rewritten as

(74)
$$\left[\begin{pmatrix} I & 0 \\ 0 & \left(\frac{1}{2}+\frac{1}{2}\frac{\varepsilon_o}{\varepsilon_i}\right) I \end{pmatrix} + \begin{pmatrix} (\varepsilon_i D0 - \varepsilon_o D1) & -(S0-S1)\,\varepsilon_o \\ (\varepsilon_i T0 - \varepsilon_o T1) & -(D2-D3)\,\varepsilon_o \end{pmatrix}\right] \begin{pmatrix} w_o \\ k_o \end{pmatrix} = \begin{pmatrix} \text{RHS of (70)} \\ \text{RHS of (73)} \end{pmatrix}.$$

7. Numerical results

In this section, we present numerical results of the proposed subtraction method. For the case of one sphere, we compare the "true solution" of the total electrostatic potential with the potential that is computed by the method here. The true solution is taken to be the Legendre polynomial expansion taken to a sufficient number of terms for it to converge [8]. Additionally, we compare the values of the much smaller quantity, the reaction field potential.

The accuracy of the results is influenced by the following factors:

- The size of the hemisphere Γ in Fig. 2 for regularization of hypersingular integrals.
- The number of terms M used in the reaction field approximation in equation (8).
- The number of terms n of the reaction field estimation to be included in the function $T(\mathbf{r},\mathbf{r}_s)$ in equation (13).
- The mesh sizes on the surface of the sphere.

In our numerical results, the mesh sizes chosen correspond to those used in our previous papers [28] and [20]. Mesh sizes "2", "4", "8", "16", "32" correspond to 8, 30, 122, 498, and 2018 total mesh points used, respectively. We chose these specific mesh sizes so comparison with previous published results could be done.

The total potential can be decomposed into the potential from the source charge and the potential from the reaction field

$$\phi(\mathbf{r}) = H(\mathbf{r}, \mathbf{r}_s) + \phi_{\text{rf}}(\mathbf{r}). \tag{75}$$

We compare results for both the total potential and the reaction field, both of which we take the true solutions as the Legendre polynomial expansion. In the numerical calculations, the reaction is estimated by image charges [8].

Next, we should note that we are solving for $w_o(\mathbf{r})$ and $\frac{\partial w_o(\mathbf{r})}{\partial \mathbf{n}}$ in the matrix equation. So in order to compare the true solution of the total potential $\phi(\mathbf{r})$ and its derivative, we use equation (16) to recover ϕ and $\frac{\partial \phi}{\partial \mathbf{n}}$.

7.1. Test 1: far source location

We first take a far away source location $\mathbf{r}_s = (0.5, 2, 0.2)$, which is 1.07 units away from the surface of the sphere, and $\varepsilon_i = 2$, $\varepsilon_o = 1$, $\lambda_o = \lambda_i = 0$. The errors in the total potential, reaction field potential, and normal derivative of potential are shown in Tables 1-3. Each table displays errors from using first or second degree basis functions, as well as the errors found by using the different subtraction options.

The reaction field potential is estimated by using $M = 16$ image charges in equation (8) while the first $n = 3$ of those terms are included in the function $T(\mathbf{r}, \mathbf{r}_s)$. The regularization hemisphere Γ has radius $a = 0.1$ units, and the true solution is calculated by the Legendre polynomial expansion out to 300 terms.

To show the effectiveness of the subtraction method, we have included what the errors are with and without its use. In Tables 1-3, the columns labeled "H subtr." and "H & T subtr." represent the cases where $T = 0$ and $H \neq T \neq 0$, respectively.

From tables 1-3, we can see that using second degree basis functions yields the better results overall as established in previous works [28], [20]. Additionally and more importantly, we see that in using either H or both H and T subtractions in the boundary integral equations, relative error is clearly improved over the case where subtraction is not utilized, proving the new technique effective in reducing the error in the potential ϕ and its derivative $\frac{d\phi}{d\mathbf{n}}$. Even in this case the potential on the sphere is not very singular due to the far away location of the source charge and the subtraction method already improved the numerical results compared with the case without subtraction.

Next we comment on the reaction field potentials. In general, the reaction field $\phi_{rf} = \phi - H$ is a much smaller quantity (in absolute value) compared to

Table 1: Relative errors of total potential in Test 1 for various mesh sizes, using first and second degree basis functions

	Relative Errors of Total Potential					
	1^{st} degree basis			2^{nd} degree basis		
mesh	no subtr	H subtr	H & T subtr	no subtr	H subtr	H & T subtr
2	0.147326	0.0451651	0.0064671	0.124979	0.0368819	0.00395786
4	0.0522389	0.0150604	0.00193832	0.0215941	0.00616589	0.000466486
8	0.0138911	0.00417494	0.000593827	0.00334666	0.000898452	0.0000323739
16	0.00569466	0.00167545	0.000193565	0.000230577	0.0000634443	4.78048×10^{-6}
32	0.00191946	0.000555919	0.0000550178	0.0000219655	5.8952×10^{-6}	2.3675×10^{-6}

Table 2: Relative errors of reaction field potential in Test 1 for various mesh sizes, using first and second degree basis functions

	Relative Errors of Reaction Field					
	1^{st} degree basis			2^{nd} degree basis		
mesh	no subtr	H subtr	H & T subtr	no subtr	H subtr	H & T subtr
2	34.3892	10.5425	1.50957	39.5287	11.5307	1.03286
4	50.716	13.2191	0.732064	28.499	8.06661	0.544632
8	8.31957	2.64289	0.59349	0.636629	0.159921	0.00669324
16	1.6258	0.549469	0.157682	0.0690341	0.0207826	0.00747426
32	1.70722	0.498056	0.111137	0.0143975	0.00454178	0.00586212

Table 3: Relative errors of normal derivative of potential in Test 1 for various mesh sizes, using first and second degree basis functions

	Relative Errors of Derivative					
	1^{st} degree basis			2^{nd} degree basis		
mesh	no subtr	H subtr	H & T subtr	no subtr	H subtr	H & T subtr
2	34.3892	0.191065	0.0273583	39.5287	0.107137	0.00967053
4	50.716	1.00924	0.0610653	28.499	0.637247	0.0403231
8	8.31957	0.215449	0.0445116	0.636629	0.122411	0.0152007
16	1.6258	0.284995	0.0573947	0.0690341	7.79×10^{-3}	1.18×10^{-3}
32	1.70722	0.083334	0.0149403	0.0143975	9.15×10^{-4}	8.25×10^{-4}

the potential from the source charge H, so getting accurate relative results is harder. We can see in Table 2 that the results using the subtraction method proposed in this paper are much improved compared to results without it. The errors for $\frac{\partial \phi}{\partial \mathbf{n}}$ are determined using 150 terms in the Legendre polynomial expansion.

7.2. Test 2: close source location

To show the effectiveness of the subtraction technique when the charge is close to the sphere, we consider a source charge 0.01 units away from the surface of the sphere, for which it is hard to accurately calculate the potential

Table 4: Relative errors of total potential in Test 2 for various mesh sizes, using first and second degree basis functions

	Relative Errors of Total Potential					
	1^{st} degree basis			2^{nd} degree basis		
mesh	no subtr	H subtr	H & T subtr	no subtr	H subtr	H & T subtr
2	0.352163	0.115115	0.0240107	0.531248	0.11688	0.0213394
4	0.482445	0.116769	0.00911358	0.44059	0.119128	0.0040248
8	0.448044	0.118087	0.00305186	0.440296	0.113837	0.00120092
16	0.440818	0.115044	9.43×10^{-4}	0.34609	0.0869985	3.01×10^{-4}
32	0.365045	0.0924509	1.95×10^{-4}	0.366269	0.0925824	3.22×10^{-5}

Table 5: Relative errors of reaction field potential in Test 2 for various mesh sizes, using first and second degree basis functions

	Relative Errors of Reaction Field					
	1^{st} degree basis			2^{nd} degree basis		
mesh	no subtr	H subtr	H & T subtr	no subtr	H subtr	H & T subtr
2	5.18242	1.69745	0.352768	43.6461	10.2175	0.986932
4	40.4081	10.1842	0.174657	80.106	21.7792	0.642631
8	80.7679	21.6078	0.448141	300.33	76.6964	0.324478
16	302.034	77.8786	0.203476	565.648	141.099	0.223372
32	626.125	158.083	0.122514	1407.16	355.185	0.0538898

and its derivative. In tables 4-6, we show the relative errors in the total potential, reaction field potential, and the normal derivative of potential. For the right-hand side integrals in (59) that are evaluated over the entire surface S, we allocate (in the standard naive, non-patch method) over 3 million Gauss points per integral in order to calculate them to sufficient accuracy.

In Table 4, we can see the use of both H and T in $w_o = \phi_o - H - T$ in the BIE's paying off, as we have a significantly lower relative error in the total potential than with having solved for just $w_o = \phi_o$. For example, we have 0.00003 relative error for mesh size 32, second degree basis functions, where the subtraction of H and T are used. This is significantly lower than the 0.36 relative error obtained by solving the BIE's without H and T.

Also, in Table 5, where we are comparing errors in the reaction field, we see that the error only converges as we take finer meshes for the second degree basis functions, with both H and T being used. Again this is because the reaction field is a much smaller quantity than the total potential. So the accuracy gathered for the total potential will always be better than the accuracy gathered for the reaction field, but it is important to demonstrate that the subtraction method is noticeably more effective for calculating this small quantity as well.

Table 6: Relative errors of derivative of potential in Test 2 for various mesh sizes, using first and second degree basis functions

	Relative Errors of Derivative					
	1^{st} degree basis			2^{nd} degree basis		
mesh	no subtr	H subtr	H & T subtr	no subtr	H subtr	H & T subtr
2	0.323243	0.116345	0.0242683	0.249254	0.183102	0.0214824
4	0.268807	0.182929	0.00916592	0.281771	0.186707	0.00483961
8	0.276892	0.18605	0.00373556	1.47951	0.700076	0.0013295
16	1.48067	0.708229	0.00442446	2.46672	0.981638	0.00216574
32	2.66079	1.09548	0.00194061	10.5346	5.57382	0.00269913

Table 7: Integrals calculated using patch method

integral	true	d=128, s=8 677888 pts	abs error
J0	0.420119962364	0.42011996239	2.6×10^{-11}
J1	-0.015986142	-0.01598671417	5.7217×10^{-7}
J3	-0.04183241584	-0.04183241586	2×10^{-11}

7.3. Results with adaptive quadrature

Now we demonstrate the effectiveness of the "patch method" adaptive quadrature.

- Integral accuracy improvement

For mesh point $(0, 0, 1)$ and source location $\mathbf{r}_s = (0.2438, 0.9752, 0.0975)$, we show results that we have gathered for the integrals $J0$, $J1$, $J2$. The top table shows the true value of the integral, gotten through Mathematica, compared to the value we calculate for the integrals in our program. The third column in Table 7 are the values we got in our program when using the patch method. The denser patches had Gauss point distributions of 128×128, with the rest of the domain grid having 8×8 distributions. This means that the total number of Gauss points over the entire integral domain is 677888 points. The last column in Table 7 is the absolute error between the values in column two (the true value) and column three (the estimated value).

The next table, Table 8, we have the true value of the integrals and the estimated value of the integrals without using the patch method in our program. The values in the third column are found by using a traditional all-over 1024×1024 distribution of Gauss points. Notice that we end up using more more Gauss points with larger error. We then see that the patch technique is more efficient and improves accuracy.

Table 8: Integrals calculated using traditional $[0, 2\pi] \times [0, \pi]$ point distribution

integral	true	1024*1024 1,048,576 pts	abs error
J0	0.420119962364	0.41999738802	1.225×10^{-4}
J1	-0.015986142	-0.016026949148	4.0807×10^{-5}
J3	-0.04183241584	-0.04175077572	8.164×10^{-5}

Table 9: Relative error of total potential in Test 2 for various mesh sizes, using second degree basis functions and refined adaptive quadrature

		Parameters			
		d=128	d=128, s=8	d=64, s=8	d = 32, s=8
pts. used per int.		3,276,800	812480	210368	59776
mesh	2	0.0213394	0.0213394	0.0211697	0.0204199
	4	0.0040248	0.00402483	0.00410833	0.0173528
	8	0.00120092	0.00120091	0.00127017	0.0216869
	16	0.000300151	0.000300154	0.000397217	0.0218253
	32	0.0000321367	0.0000320931	0.000285613	0.0218124

- **Test 2 revisited** with adaptive quadratures on right handside integrals

  For the source location

$$\mathbf{r}_s = (0.2438162975, 0.9752651902, 0.097526519),$$

which is 0.01 units away from the surface of the sphere, we compare our previous results in Test 2 with results found by patch method. The overall parameters are the same as in Test 2: $\varepsilon_i = 2$, $\varepsilon_o = 1$, $\lambda_o = \lambda_i = 0$, $M = 16$, $n = 3$, $a = 0.1$. Additionally, we have four integrals, $J0$, $J1$, $J3$, $J4$ over large domains of the integration geometry, for which we employ the patch method technique, using a 10×20 grid giving 200 patches. As the other four integrals are evaluated over a small region, we simply assign a dense spread of Gauss points distributed in the traditional way.

Table 9 shows the relative errors gotten for the total potential using a second degree basis for the mesh. Table 10 shows the relative errors in the reaction field using a second degree basis. The first columns of the tables are errors reported in Tables 4, 5, and 6. The successive columns in these tables show the relative errors in the respective quantities obtained by the patch method on the four right-hand side integrals. For column two in Tables 9 and 10, the denser patches have 128×128 Gauss points per patch, and the rest of the patches have 8×8 points per patch. In column three, the denser patches have 64×64 Gauss points per patch.

Table 10: Relative error of reaction field for mesh sizes 2, 4, 8, 16, 32 using second degree basis and refined quadrature

		Parameters			
		d=128	d=128, s=8	d=64, s=8	d = 32, s=8
pts. used per int.		3,276,800	812480	210368	59776
mesh	2	0.986932	0.986931	0.98656	0.999572
	4	0.642631	0.642628	0.64101	0.452381
	8	0.324478	0.324477	0.339294	2.006
	16	0.223372	0.223351	0.227471	3.0974
	32	0.0538898	0.0539396	0.0816155	6.55852

Table 11: Relative error of normal derivative of potential in Test 2 for various mesh sizes, using second degree basis functions and refined adaptive quadrature

		Parameters			
		d=128	d=128, s=8	d=64, s=8	d = 32, s=8
pts. used per int.		3,276,800	812480	210368	59776
mesh	2	0.0214824	0.0214824	0.0213114	0.0205538
	4	0.00483961	0.00483961	0.00483858	0.0175223
	8	0.0013295	0.00132949	0.00134285	0.0305661
	16	0.00216574	0.00216556	0.00272643	0.174483
	32	0.00269913	0.00269691	0.00804604	0.805969

Table 12: Relative error of total potential, reaction field potential, and derivative of potential for mesh sizes 2, 4, 8, 16, 32 in Test 3, using second degree basis

mesh size	2	4	8	16	32
tot. pot.	0.017975	0.00267459	0.000756977	0.0000834943	$4.75117 * 10^{-6}$
r.f.	0.837977	0.405549	0.239895	0.051579	0.00334053
der.	0.018093	0.00309373	0.00084127	0.00112238	0.00297702

These tables demonstrate how few total Gauss points we could use and still get the good results that we calculated previously. We can see for both the total potential and the reaction field potential, for this particular example and setup, anything below 210368 total Gauss points on those four integrals would generate unacceptable errors, but any amount above that number is sufficient and at a significantly reduced cost compared to the traditional calculation in column one.

- **Test 3** (refined adaptive quadrature)

Table 13: Relative error of total potential in Test 3 for various mesh sizes, using second degree basis functions and refined adaptive quadrature

		Parameters		
		d=128, s=8	d_1=128, d_2 = 77, s=8	d_1 = 128, d_2 = 64, s=8
pts per int.		812480	394280	320960
mesh	2	0.017975	0.0179753	0.0179687
	4	0.00267459	0.00267457	0.00267348
	8	0.000756977	0.000750166	0.000826218
	16	0.0000834943	0.0000847098	0.000267764
	32	4.76×10^{-6}	0.0000517394	0.000241497

Table 14: Relative error of reaction field potential in Test 3 for various mesh sizes, using second degree basis functions and refined adaptive quadrature

		Parameters		
		d=128, s=8	d_1=128, d_2 = 77, s=8	d_1 = 128, d_2 = 64, s=8
pts per int.		812480	394280	320960
mesh	2	0.837977	0.838036	0.837387
	4	0.405549	0.405582	0.405224
	8	0.239895	0.239966	0.242313
	16	0.051579	0.0515831	0.0531272
	32	0.00334053	0.00330263	0.00351808

Based on the way we set up the patch method technique for the right-hand side integrals in the matrix equation (59), when we choose a domain grid size of $p \times q$, then a total of $9 + 2q$ patches have denser Gauss point coverage; nine patches are around the projection of the source point onto the sphere, $\mathbf{r}'_s$, and $2q$ patches are around the mesh point $\mathbf{p}$.

When we revisited Test 2 earlier, we use a domain grid size of 10×20, resulting in 200 total patches over which the domain is divided. Out of those 200, 49 of those patches have the denser coverage of Gauss points. So in this case, $2q$ equals 40, which is a substantially higher number of patches used around the mesh point $\mathbf{p}$ than the nine used for $\mathbf{r}'_s$. The extra number of patches around the mesh point $\mathbf{p}$ happens due to decreasing size of the patches around it. Therefore, we use fewer Gauss points for the smaller patches. So, in the example we've been discussing, if we use M total Gauss points in the nine patches about $\mathbf{r}'_s$, we aim to use close to M number of total points in the 40 patches about the mesh point $\mathbf{p}$.

Tables 13 through 15 contain results previously shown, where $d = 128$, $s = 8$ (dense patches are $d \times d$ and smaller-density patches are $s \times s$). The value d_1 corresponds to the density of the patches around $\mathbf{r}'_s$, and the value d_2 corresponds to the density of the patches around mesh point $\mathbf{p}$. The "points

Table 15: Relative error of normal derivative of potential in Test 3 for various mesh sizes, using second degree basis functions and refined adaptive quadrature

		Parameters		
		d=128, s=8	d_1=128, d_2 = 77, s=8	d_1 = 128, d_2 = 64, s=8
pts per int.		812480	394280	320960
mesh	2	0.018093	0.0180934	0.0180867
	4	0.00309373	0.00309269	0.00309812
	8	0.00084127	0.000843043	0.00184551
	16	0.00112238	0.00152123	0.00202031
	32	0.00297702	0.00275704	0.00859556

used per integral" row indicates how many total Gauss points are necessary to calculate the four difficult right-hand-side integrals in matrix equation (59) for which this "patch method" is meant to improve results. All other integrals are calculated using far fewer Gauss points, as the dense coverage is not needed for those.

7.4. Numerical results for two spheres

In this section, we apply the new boundary integral equations to a system of spheres. After we test the code on the case of two dielectric spheres with one of them having the same dielectric constant as the background material, it reproduces the potential of one dielectric sphere. Then we consider two cases where the second sphere has a slightly perturbed dielectric constant from the background, and compare the resulting potentials to the analytical results of one sphere as a reference. We expect the differences are in proportion to the perturbation in the dielectric constant of the second sphere.

- **Test 4**, two close spheres with source close to one sphere

In this test, we have two dielectric spheres separated, with the second dielectric sphere 0.1 units away, the first sphere having a relative dielectric constant of $\varepsilon_{1i} = 2$ and the second sphere having $\varepsilon_{2i} = 1.01$. We also assume that $\lambda_o = \lambda_{1_i} = \lambda_{2_i} = 0$. The number of images used in the subtraction are $M = 16$, and we have that $n = 3$, $a = 0.1$, the source location is close to the sphere, $\mathbf{r}_s = (0.2438162975, 0.9752651902, 0.097526519)$, and the true solution for the mesh points on sphere 1 is found by the Legendre polynomial expansion. Figures 8 and 9 illustrate the potential $\phi(\mathbf{r})$ and $\phi(\mathbf{r}) - H(\mathbf{r}, \mathbf{r}_s)$ for this system. Notice by using the subtraction in Figure 9 as the solved-for variable in our boundary integral equations, we are solving for a smoother

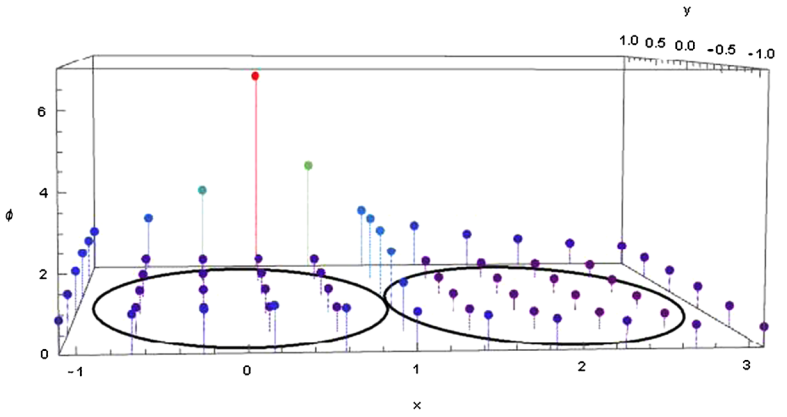

Figure 8: Electric potential $|\phi|$ for points along $z = 0$ using mesh size 2x2x2 in Test 4.

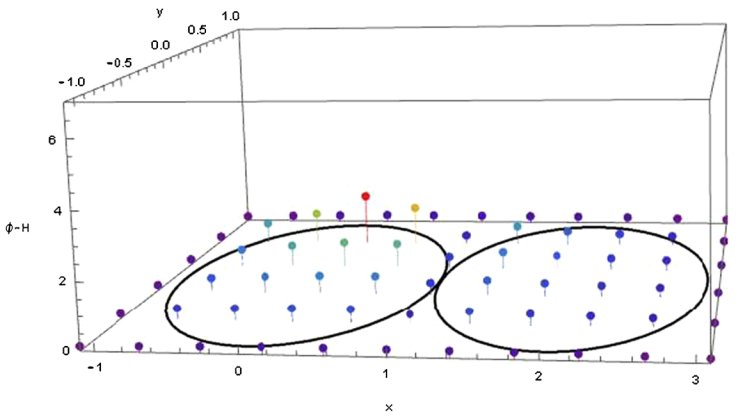

Figure 9: Electric potential $|\phi - H|$ for points along $z = 0$ using mesh size 2x2x2 in Test 4.

and smaller value. This is what gives our methods outlined in this paper their effectiveness and results in our higher accuracy for the potential and its normal derivative.

The absolute errors shown in Table 16 is the maximum difference between the BIE-calculated potential results on the first-sphere for the perturbed system shown in Figure 10 and the values of the Legendre polynomial solution of the non-perturbed system. The second column in Table 16 lists the CPU times in seconds that it took to calculate the potential and normal derivative at the mesh points for the increasingly course meshes.

Table 16: total potential absolute errors for mesh points on first sphere in Test 4

	Errors in potential		CPU total time	
	1^{st} Degree	2^{nd} Degree	1^{st} Degree	2^{nd} Degree
Mesh	Abs. Error	Abs. Error	seconds	seconds
2	2.04×10^{-2}	1.73×10^{-2}	54	180
4	6.96×10^{-3}	7.58×10^{-3}	210	797
8	6.85×10^{-3}	4.07×10^{-3}	857	3578
16	3.37×10^{-3}	2.74×10^{-3}	3714	15952
32	8.54×10^{-4}	2.68×10^{-3}	18615	93195

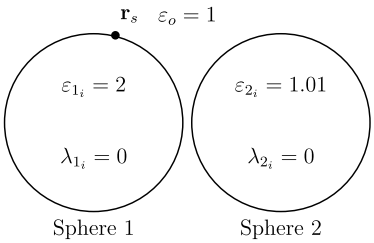

Figure 10: To-scale illustration of interaction in Test 4.

- **Test 5**, two close sphere with a source charge in between the spheres

In this case, we consider the situation where the source point is placed right in the middle of the two spheres, which gives the most singular potential. We have that $\lambda_o = \lambda_{1_i} = \lambda_{2_i} = 0$, $M = 16$, $n = 3$, $a = 0.1$, $\mathbf{r}_s = (1.05, 0, 0.2)$. The second sphere is located 0.1 units away from the first, with a perturbation in its dielectric constant of 0.1, and the source charge is located midway between those two dielectric spheres, at approximately 0.07 units distance.

The difference between the solution of the two-spheres system and one sphere only is in proportion to the perturbation of the dielectric constant of the second sphere. As the mesh is refined, the difference converges showing the numerical convergence of the method.

8. Conclusion

In this paper, we introduce an efficient and accurate integral equation method to compute the singular potential field in a closely packed charge-dielectric sphere system. A subtraction technique based de-singularization technique is used to remove the singular part of the potential where the primary Coulomb potential and reaction field (approximated by image charges) are removed

Table 17: total potential absolute errors for mesh points on first sphere in Test 5

	Two-sphere system		CPU total time	
	1^{st} Degree	2^{nd} Degree	1^{st} Degree	2^{nd} Degree
Mesh	Abs. Error	Abs. Error	seconds	seconds
2	1.95×10^{-1}	1.56×10^{-1}	74	233
4	1.78×10^{-1}	2.30×10^{-1}	269	1015
8	3.04×10^{-1}	2.15×10^{-1}	1094	4374
16	2.52×10^{-1}	2.13×10^{-1}	4614	19162
32	2.41×10^{-1}	2.14×10^{-1}	21206	97773

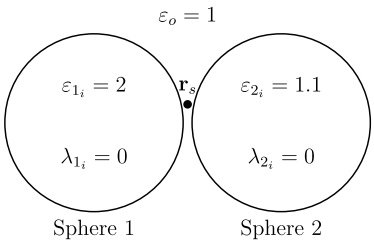

Figure 11: To-scale illustration of interaction in Test 5.

from the potential. Regularization technique for the Hadamard finite part integral is also introduced for the second kind integral equations. Numerical results for single and double spheres have validated the effectiveness of the proposed method where much higher accuracy for the singular potential can be obtained with coarse meshes, dramatically reducing the computational cost for closely packed charge-sphere systems.

Future work will include extending this technique to Janus particles and integrating the potential calculation into molecular dynamics simulations of colloidal systems of dielectric spheres [1] and Janus particles [25].

Appendix

A crucial step in the regularization of the hyper-singular integral is the use of $v(\mathbf{r}) - H(\mathbf{r}, \mathbf{r}_s) - T(\mathbf{r}, \mathbf{r}_s)$ as being of order $O(|\mathbf{r} - \mathbf{p}|)$. This reduced the integral from being hypersingular to being strongly singular. We will prove this property here. From the definitions, we have that

$$v(\mathbf{r}) = C \frac{e^{-\lambda_i |\mathbf{r}-\mathbf{z}|}}{\varepsilon_{in} |\mathbf{r} - \mathbf{z}|} \tag{76}$$

$$H(\mathbf{r}) = 4\pi G_o(\mathbf{r}, \mathbf{r}_s) = \frac{e^{-\lambda_o|\mathbf{r}-\mathbf{r}_s|}}{\varepsilon_o|\mathbf{r}-\mathbf{r}_s|} \tag{77}$$

$$T(\mathbf{r}, \mathbf{r}_s) = \frac{q_k e^{-\lambda_o|\mathbf{r}-\mathbf{r}_k|}}{\varepsilon_o|\mathbf{r}-\mathbf{r}_k|} + \frac{q_1 e^{-\lambda_o|\mathbf{r}-\mathbf{x}_1|}}{\varepsilon_o|\mathbf{r}-\mathbf{x}_1|} + \frac{q_2 e^{-\lambda_o|\mathbf{r}-\mathbf{x}_2|}}{\varepsilon_o|\mathbf{r}-\mathbf{x}_2|} \tag{78}$$

We require that

$$v(\mathbf{p}) = H(\mathbf{p}, \mathbf{r}_s) + T(\mathbf{p}, \mathbf{r}_s)$$

which gives

$$\begin{aligned} C =& \left(\frac{\varepsilon_i|\mathbf{p}-\mathbf{z}|}{\varepsilon_o|\mathbf{p}-\mathbf{r}_s|} e^{\lambda_i|\mathbf{p}-\mathbf{z}|-\lambda_o|\mathbf{p}-\mathbf{r}_s|} + \frac{q_k\varepsilon_i|\mathbf{p}-\mathbf{z}|}{\varepsilon_o|\mathbf{p}-\mathbf{r}_k|} e^{\lambda_i|\mathbf{p}-\mathbf{z}|-\lambda_o|\mathbf{p}-\mathbf{r}_k|} \right. \\ & \left. + \frac{q_1\varepsilon_i|\mathbf{p}-\mathbf{z}|}{\varepsilon_o|\mathbf{p}-\mathbf{x}_1|} e^{\lambda_i|\mathbf{p}-\mathbf{z}|-\lambda_o|\mathbf{p}-\mathbf{x}_1|} + \frac{q_2\varepsilon_i|\mathbf{p}-\mathbf{z}|}{\varepsilon_o|\mathbf{p}-\mathbf{x}_2|} e^{\lambda_i|\mathbf{p}-\mathbf{z}|-\lambda_o|\mathbf{p}-\mathbf{x}_2|} \right). \end{aligned} \tag{79}$$

Therefore

$$v(\mathbf{r}) = \frac{e^{-\lambda_o|\mathbf{p}-\mathbf{r}_s|}}{\varepsilon_o|\mathbf{p}-\mathbf{r}_s|} + \frac{q_k e^{-\lambda_o|\mathbf{p}-\mathbf{r}_k|}}{\varepsilon_o|\mathbf{p}-\mathbf{r}_k|} + \frac{q_1 e^{-\lambda_o|\mathbf{p}-\mathbf{x}_1|}}{\varepsilon_o|\mathbf{p}-\mathbf{x}_1|} + \frac{q_1 e^{-\lambda_o|\mathbf{p}-\mathbf{x}_2|}}{\varepsilon_o|\mathbf{p}-\mathbf{x}_2|}.$$

Because $\mathbf{p}$ and $\mathbf{r}$ are both on the surface S of the sphere of radius 1 whose center is $\mathbf{z}$, the quantity inside the parentheses is 1. Now we consider the difference

$$\begin{aligned} |v(\mathbf{r}) - H(\mathbf{r}, \mathbf{r}_s) - T(\mathbf{r}, \mathbf{r}_s)| =& \left| \frac{e^{-\lambda_o|\mathbf{p}-\mathbf{r}_s|}}{\varepsilon_o|\mathbf{p}-\mathbf{r}_s|} + \frac{q_k e^{-\lambda_o|\mathbf{p}-\mathbf{r}_k|}}{\varepsilon_o|\mathbf{p}-\mathbf{r}_k|} + \frac{q_1 e^{-\lambda_o|\mathbf{p}-\mathbf{x}_1|}}{\varepsilon_o|\mathbf{p}-\mathbf{x}_1|} \right. \\ & + \frac{q_1 e^{-\lambda_o|\mathbf{p}-\mathbf{x}_2|}}{\varepsilon_o|\mathbf{p}-\mathbf{x}_2|} - \frac{e^{-\lambda_o|\mathbf{r}-\mathbf{r}_s|}}{\varepsilon_o|\mathbf{r}-\mathbf{r}_s|} - \frac{q_k e^{-\lambda_o|\mathbf{r}-\mathbf{r}_k|}}{\varepsilon_o|\mathbf{r}-\mathbf{r}_k|} - \frac{q_1 e^{-\lambda_o|\mathbf{r}-\mathbf{x}_1|}}{\varepsilon_o|\mathbf{r}-\mathbf{x}_1|} \\ & \left. - \frac{q_2 e^{-\lambda_o|\mathbf{r}-\mathbf{x}_2|}}{\varepsilon_o|\mathbf{r}-\mathbf{x}_2|} \right| \\ =& \left| \left(\frac{e^{-\lambda_o|\mathbf{p}-\mathbf{r}_s|}}{\varepsilon_o|\mathbf{p}-\mathbf{r}_s|} - \frac{e^{-\lambda_o|\mathbf{r}-\mathbf{r}_s|}}{\varepsilon_o|\mathbf{r}-\mathbf{r}_s|} \right) + \left(\frac{q_k e^{-\lambda_o|\mathbf{p}-\mathbf{r}_k|}}{\varepsilon_o|\mathbf{p}-\mathbf{r}_k|} - \frac{q_k e^{-\lambda_o|\mathbf{r}-\mathbf{r}_k|}}{\varepsilon_o|\mathbf{r}-\mathbf{r}_k|} \right) \right. \\ & + \left(\frac{q_1 e^{-\lambda_o|\mathbf{p}-\mathbf{x}_1|}}{\varepsilon_o|\mathbf{p}-\mathbf{x}_1|} - \frac{q_1 e^{-\lambda_o|\mathbf{r}-\mathbf{x}_1|}}{\varepsilon_o|\mathbf{r}-\mathbf{x}_1|} \right) \\ & \left. + \left(\frac{q_1 e^{-\lambda_o|\mathbf{p}-\mathbf{x}_2|}}{\varepsilon_o|\mathbf{p}-\mathbf{x}_2|} - \frac{q_2 e^{-\lambda_o|\mathbf{r}-\mathbf{x}_2|}}{\varepsilon_o|\mathbf{r}-\mathbf{x}_2|} \right) \right| \end{aligned} \tag{80}$$

For each of the terms in parentheses above, we will need the Taylor expression of $f(\mathbf{r}) = \frac{e^{-\lambda|\mathbf{r}-\mathbf{r}_j|}}{\mathbf{r}-\mathbf{r}_j}$ centered at $\mathbf{p}$, for source or image point $\mathbf{r}_j$. Let D be the

gradient and D^2 be the Hessian matrix. Assuming all vectors are transposed for the appropriate inner product, the Taylor expansion is given by

$$f(\mathbf{r}) + (\mathbf{r}-\mathbf{p}) \cdot Df(\mathbf{p}) + (\mathbf{r}-\mathbf{p}) \cdot D^2 f(\mathbf{p}) \cdot (\mathbf{r}-\mathbf{p})/2 + \cdots . \tag{81}$$

For completeness, first consider $f(\mathbf{r}) = \exp(-\lambda|\mathbf{r}-\mathbf{r}_j|)$. Then

$$f(\mathbf{p}) = e^{-\lambda|\mathbf{p}-\mathbf{r}_j|}, \tag{82}$$

$$Df(\mathbf{p}) = -\frac{\mathbf{p}-\mathbf{r}_j}{|\mathbf{p}-\mathbf{r}_j|}\lambda e^{-\lambda|\mathbf{p}-\mathbf{r}_j|}, \tag{83}$$

(84)
$$D^2 f(\mathbf{p}) = \left[\frac{(\mathbf{p}-\mathbf{r}_j)\otimes(\mathbf{p}-\mathbf{r}_j)}{|\mathbf{p}-\mathbf{r}_j|^2}\left(\lambda - \frac{1}{|\mathbf{p}-\mathbf{r}_j|}\right) + I\frac{1}{|\mathbf{p}-\mathbf{r}_j|}\right]\lambda e^{-\lambda|\mathbf{p}-\mathbf{r}_j|}.$$

In the Hessian matrix D^2, $\otimes$ is the outer product and I is the identity matrix. The Taylor expansion, ignoring truncation error, of $f(\mathbf{r}) = \exp(-\lambda|\mathbf{r}-\mathbf{r}_j|)$ can be written as

$$\begin{aligned} f(\mathbf{r}) &= e^{-\lambda|\mathbf{p}-\mathbf{r}_j|} - (\mathbf{r}-\mathbf{p}) \cdot \frac{\mathbf{p}-\mathbf{r}_j}{|\mathbf{p}-\mathbf{r}_j|}\lambda e^{-\lambda|\mathbf{p}-\mathbf{r}_j|} \\ &+ (\mathbf{r}-\mathbf{p}) \cdot \left[\frac{(\mathbf{p}-\mathbf{r}_j)\otimes(\mathbf{p}-\mathbf{r}_j)}{|\mathbf{p}-\mathbf{r}_j|^2}\left(\lambda - \frac{1}{|\mathbf{p}-\mathbf{r}_j|}\right)\right. \\ &\left. + I\frac{1}{|\mathbf{p}-\mathbf{r}_j|}\right]\lambda e^{-\lambda|\mathbf{p}-\mathbf{r}_j|} \cdot (\mathbf{r}-\mathbf{p})/2. \end{aligned} \tag{85}$$

Now let $f(\mathbf{r}) = \exp(-\lambda|\mathbf{r}-\mathbf{r}_j|)/|\mathbf{r}-\mathbf{r}_j|$. Repeating the process, we first need

$$f(\mathbf{p}) = \frac{e^{-\lambda|\mathbf{p}-\mathbf{r}_j|}}{|\mathbf{p}-\mathbf{r}_j|}, \tag{86}$$

$$Df(\mathbf{p}) = -\frac{\mathbf{p}-\mathbf{r}_j}{|\mathbf{p}-\mathbf{r}_j|}\left(\lambda - \frac{1}{|\mathbf{p}-\mathbf{r}_j|}\right)\frac{e^{-\lambda|\mathbf{p}-\mathbf{r}_j|}}{|\mathbf{p}-\mathbf{r}_j|}, \tag{87}$$

$$\begin{aligned} D^2 f(\mathbf{p}) = \left[\frac{(\mathbf{p}-\mathbf{r}_j)\otimes(\mathbf{p}-\mathbf{r}_j)}{|\mathbf{p}-\mathbf{r}_j|^2}\left(3\lambda + \frac{\lambda^2}{|\mathbf{p}-\mathbf{r}_j|} + \frac{3}{|\mathbf{p}-\mathbf{r}_j|^3}\right)\right. \\ \left. - I\left(\frac{\lambda}{|\mathbf{p}-\mathbf{r}_j|} + \frac{1}{|\mathbf{p}-\mathbf{r}_j|^3}\right)\right] e^{-\lambda|\mathbf{p}-\mathbf{r}_j|}. \end{aligned} \tag{88}$$

The Taylor expansion, ignoring truncation error, of $f(\mathbf{r}) = \exp(-\lambda|\mathbf{r}-\mathbf{r}_j|)/|\mathbf{r}-\mathbf{r}_j|$ can be written as

$$\begin{aligned}\frac{f(\mathbf{r})}{|\mathbf{r}-\mathbf{r}_j|} &= \frac{e^{-\lambda|\mathbf{p}-\mathbf{r}_j|}}{|\mathbf{p}-\mathbf{r}_j|} - (\mathbf{r}-\mathbf{p})\cdot\frac{\mathbf{p}-\mathbf{r}_j}{|\mathbf{p}-\mathbf{r}_j|}\left(\lambda - \frac{1}{|\mathbf{p}-\mathbf{r}_j|}\right)\frac{e^{-\lambda|\mathbf{p}-\mathbf{r}_j|}}{|\mathbf{p}-\mathbf{r}_j|} \\ &+ (\mathbf{r}-\mathbf{p})\cdot\left[\frac{(\mathbf{p}-\mathbf{r}_j)\otimes(\mathbf{p}-\mathbf{r}_j)}{|\mathbf{p}-\mathbf{r}_j|^2}\left(3\lambda + \frac{\lambda^2}{|\mathbf{p}-\mathbf{r}_j|} + \frac{3}{|\mathbf{p}-\mathbf{r}_j|^3}\right)\right. \\ &\left. -I\left(\frac{\lambda}{|\mathbf{p}-\mathbf{r}_j|} + \frac{1}{|\mathbf{p}-\mathbf{r}_j|^3}\right)\right] e^{-\lambda|\mathbf{p}-\mathbf{r}_j|}\cdot(\mathbf{r}-\mathbf{p})/2. \qquad (89)\end{aligned}$$

Using only the approximation $f(\mathbf{r}) = f(\mathbf{p}) + (\mathbf{r}-\mathbf{p})\cdot Df(\mathbf{p})$ by ignoring the Hessian for $\exp(-\lambda|\mathbf{r}-\mathbf{r}_j|)/|\mathbf{r}-\mathbf{r}_j|$, the difference for $|v(\mathbf{r}) - H(\mathbf{r}) - T(\mathbf{r},\mathbf{r}_s)|$ is

$$\begin{aligned}|v(\mathbf{r}) - H(\mathbf{r}) - T(\mathbf{r},\mathbf{r}_s)| = &\left[\left((\mathbf{r}-\mathbf{p})\cdot\frac{\mathbf{p}-\mathbf{r}_s}{|\mathbf{p}-\mathbf{r}_s|}\left(\lambda - \frac{1}{|\mathbf{p}-\mathbf{r}_s|}\right)\frac{e^{-\lambda|\mathbf{p}-\mathbf{r}_s|}}{|\mathbf{p}-\mathbf{r}_s|}\right)\right. \\ &+ \left((\mathbf{r}-\mathbf{p})\cdot\frac{\mathbf{p}-\mathbf{r}_k}{|\mathbf{p}-\mathbf{r}_k|}\left(\lambda - \frac{1}{|\mathbf{p}-\mathbf{r}_k|}\right)\frac{e^{-\lambda|\mathbf{p}-\mathbf{r}_k|}}{|\mathbf{p}-\mathbf{r}_k|}\right) \\ &+ \left((\mathbf{r}-\mathbf{p})\cdot\frac{\mathbf{p}-\mathbf{x}_1}{|\mathbf{p}-\mathbf{x}_1|}\left(\lambda - \frac{1}{|\mathbf{p}-\mathbf{x}_1|}\right)\frac{e^{-\lambda|\mathbf{p}-\mathbf{x}_1|}}{|\mathbf{p}-\mathbf{x}_1|}\right) \\ &\left. + \left((\mathbf{r}-\mathbf{p})\cdot\frac{\mathbf{p}-\mathbf{x}_2}{|\mathbf{p}-\mathbf{x}_2|}\left(\lambda - \frac{1}{|\mathbf{p}-\mathbf{x}_2|}\right)\frac{e^{-\lambda|\mathbf{p}-\mathbf{x}_2|}}{|\mathbf{p}-\mathbf{x}_2|}\right)\right] \\ = &\, O(\mathbf{r}-\mathbf{p})\end{aligned}$$

Acknowledgments

The work of this research was supported by US Army Research Office (Grant No. W911NF-17-1-0368) and US National Science Foundation (Grant No. DMS-1802143).

References

[1] K. Barros, E. Luijten. Dielectric Effects in the Self-Assembly of Binary Colloidal Aggregates. *Physical Review Letters. PRL* **113**, 017801, 2014.

[2] A.A. Becker. *The Boundary Element Method in Engineering: A Complete Course*. McGraw-Hill, 1992.

[3] C.A. Brebbia, J. Dominguez. *Boundary Elements: An Introductory Course*, 2nd Ed. Computational Mechanics Publications, 1992. MR1169462

[4] C.A. Brebbia, J. Dominguez. Boundary element methods for potential problems. *Applied Mathematical Modelling* **1**, 372–378, 1977. MR0520348

[5] C.A. Brebbia, J.C.F. Telles, L.C. Wrobel. *Boundary Element Techniques, Theory and Applications in Engineering*. Springer-Verlag, Berlin, Heidelberg, 1984.

[6] C.A. Brebbia. *Progress in Boundary Element Methods*, Vol. 1. Oxford University Press, 1981. MR0732950

[7] W. Cai. *Computational Methods for Electromagnetic Phenomena*, First Ed. Cambridge University Press, New York, 2013. MR3027264

[8] W. Cai, Shaozhong Deng, Donald Jacobs. Extending the fast multipole method to charges inside or outside a dielectric sphere. *Journal of Computational Physics* **223**, 846–864, 2007. MR2319236

[9] L. Chen, M. Holst, J. Xu. The finite element approximation of the nonlinear Poisson–Boltzmann equation. *SIAM J. Numer. Anal.* **45**, 2298–2320, 2007. MR2361891

[10] I.-L. Chern, J.G. Liu, W.-C. Wang. Accurate evaluation of electrostatics for macromolecules in solution. *Meth. Appl. Anal.* **10**, 309–328, 2003. MR2074754

[11] P.G. Ciarlet. *The Finite Element Method for Elliptic Problems*. North Holland Publishing, Amsterdam, 1978. MR0520174

[12] M.E. Davis, J.A. McCammon. Solving the finite difference linearized Poisson-Boltzmann equation: A comparison of relaxation and conjugate gradient methods. *Journal of Computational Chemistry* **10**, 3, 386–391, 1989.

[13] S. Deng, W. Cai. Extending the fast multipole method for charges inside a dielectric sphere in an ionic solvent: High-order image approximations for reaction fields. *Journal of Computational Physics*, 1246–1266, 2007. MR2442394

[14] F. Fogolari, A. A. Brigo, H. Molinari. The Poisson-Boltzmann equation for biomolecular electrostatics: a tool for structural biology. *J. Mol. Recognit.*, 377–392, 2002.

[15] M. Holst, N. Baker, F. Wang. Adaptive multilevel finite element solution of the Poisson–Boltzmann equation I. Algorithms and examples. *Journal of Computational Chemistry* **21**, 15, 1319–1342, 2000.

[16] A.H. Juffer, E.F.F. Botta, B.A.M. van Keulen, A. van der Ploeg, H.J.C. Berendsen. The electric potential of a macromolecule in a solvent: A fundamental approach. *J. Comput. Phys.* **97**, 144–171, 1991.

[17] J.C. Lachat, J.O. Watson. Effective numerical treatment of boundary integral equations: a formulation for three-dimensional elastostatics. *Int. J. Numer. Meth. Eng.* **10**, 991–1005, 1976.

[18] Z. Li, K. Ito. The Immersed Interface Method: Numerical Solutions of PDEs Involving Interfaces and Irregular Domains. SIAM, Philadelphia, PA, 2006. MR2242805

[19] H. Lin, H. Tang, Wei Cai. Accuracy and efficiency in computing electrostatic potential for an ion channel model in layered dielectric/electrolyte media. *Journal of Computational Physics*, 448–512, 2013.

[20] H.M. Lin, Z.L. Xu, H.Z. Tang, W. Cai. Image Approximations to Electrostatic Potentials in Layered Electrolytes/Dielectrics and an Ion-Channel Model. *The Journal of Scientific Computing*, DOI 10.1007/s10915-011-9567-2, 2011. MR2983093

[21] B. Lu, D. Zhang, J.A. McCammon. Computation of electrostatic forces between solvated molecules determined by the Poisson–Boltzmann equation using a boundary element method. *The Journal of Chemical Physics* **122**, 21, DOI 10.1063/1.1924448, 2005.

[22] B. Lu, Y.C. Zhou, M.J. Holst, J.A. McCammon. Recent progress in numerical methods for the Poisson-Boltzmann equation in biophysical applications. *Communications in Computational Physics* **3**, 973–1009, 2008.

[23] R.P. Sheridan, R.M. Levy, F.R. Salemme. Alpha-Helix dipole model and electrostatic stabilization of 4-alpha-helical proteins. *Proceedings of the National Academy of Sciences of the Unites States of America* **79**, 15, 4545–4549, 1982.

[24] W.C. Still, A. Tempczyk, R.R. Hawkley, T. Hendrickson. Semianalytical treatment of solvation for molecular mechanics and dynamics. *Journal of the American Chemical Society*, 6127–6129, 1990.

[25] A. Walther, A.H.E. Müller. Janus Particles: Synthesis, Self-Assembly, Physical Properties and Applications. *Chemical Reviews*, 5194–5261, 2013.

[26] Z.L. Xu, W. Cai. Fast analytical methods for macroscopic electrostatic models in biomolecular simulations. *SIAM Review*, 683–720, 2011. MR2861263

[27] C.H. Yan, W. Cai, X. Zeng. A parallel method for solving Laplace equations with Dirichlet data using local boundary integral equations and random walks. *SIAM J. Scientific Computing* **35**, 4, B868–B889, 2013. MR3090159

[28] B. Zinser, W. Cai. A well-conditioned hypersingular boundary element method for electrostatic potentials in the presence of inhomogeneities within layered media. *Communication in Computational Physics* **19**, 4, 970–997, 2016. MR3514243

Caylah Retz
Department of Mathematics
University of North Carolina at Charlotte
Charlotte NC 28223
USA

Wei Cai
Department of Mathematics
Southern Methodist University
Dallas TX 75275
USA
E-mail: cai@smu.edu
Phone: 214-768-3320